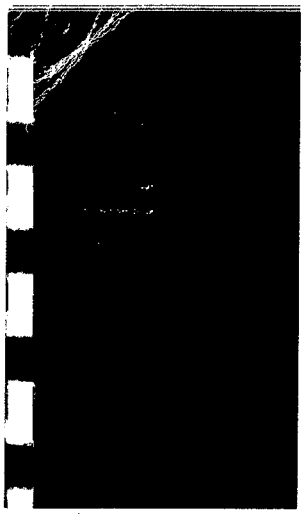

Cranfield UNIVERSITY

The stability and control characteristics of the neutrally bouyant non-rigid airship

F.Goineau
M.V.Cook

COA report No.9911
August 1999

Flight Test and Dynamics Group
College of Aeronautics
Cranfield University
Cranfield
Bedford MK43 0AL
England

College of Aeronautics Report No.9911
August 1999

The stability and control characteristics of the neutrally bouyant non-rigid airship

F.Goineau
M.V.Cook

ISBN 1861940459

Flight Test and Dynamics Group
College of Aeronautics
Cranfield University
Cranfield
Bedford MK43 0AL
England

ABSTRACT

The response to controls of a neutrally buoyant non-rigid airship was investigated for a range of speeds from the hover to 30 m/s using a non-linear simulation model. The responses shown include both flight path and a range of motion variables. The latter show the influence of the stability modes on control. The controls included in the airship model comprise equivalent elevator, equivalent rudder, thrust magnitude and thrust vector direction.

A linearised state model of the airship was obtained from the simulation model for a range of speeds from the hover to 30 m/s. The validity of the linearised model for short term evaluation of stability and control was confirmed by matching linear response plots with those obtained from the simulation model. By making assumptions about the nature of response, the state equations were simplified to enable algebraic approximations for the stability modes to be derived by analysis. The approximate models were shown to compare favourably with the actual modes obtained in the solution of the equations of motion.

CONTENTS

1. Introduction

The airship provided the first practical means for trans-global travel and during the 1920's and 1930's a number of very large rigid airships were developed for that purpose. At that time, the very highly flammable hydrogen gas, being the lightest gas available in sufficient quantities, was used to provide buoyancy. Over the years, a number of high profile accidents involving the airship did not help its cause. In particular, the loss of the Hindenburg in a spectacular fire in 1937 raised serious questions about the role of the airship for passenger carrying services. Since large transport aircraft were developing rapidly the demise of the large commercial airship was not surprising.

In more recent years there has been a resurgence of interest in the airship for commercial applications. The ready availability of inert helium gas in sufficient quantities, the development of modern lightweight gas-tight materials and the relative simplicity of a non-rigid structure, together make a modern commercial airship an attractive proposition. A number of manufacturers are convinced that a market exists for the unique operational advantages that can only be provided by the airship. Thus a small, but significant, number of modern airship developments continue to be pursued by various organisations around the world.

By the early 1980's Airship Industries Ltd. in the UK had developed and successfully flown the Skyship 500 and 600 series of non-rigid airships. The undoubted success of these airships was due, in part, to the significant use of very advanced materials and manufacturing techniques in their construction. The ultimate achievement by the company was the development of a demonstrator airship with optically signalled flying controls, claimed to be the worlds' first fly-by-light control system. Trials reports indicated that the control characteristics of the demonstrator were far superior to those of the mechanically controlled airship.

In the mid-1980's Airship Industries Ltd. was awarded a contract by the US Department of Defense to develop a very large non-rigid airship for the US Coast Guard Service. The YEZ-2A airship was more than twice the size of existing machines and was intended for a very long endurance surveillance role. In turn, the College of Aeronautics was sub-contracted by Airship Industries Ltd. to undertake an extensive series of wind tunnel tests and to contribute to the development of an aerodynamic model of the YEZ-2A. This work was undertaken by Gomes[1] who eventually used the aerodynamic model to study the dynamics, stability and control of the non-rigid airship. A short time later a further study was undertaken by Crawford[2] in which the computer simulation model developed by Gomes was used to investigate flying and handling qualities.

Following the discovery of a minor error in the wind tunnel data reduction software, the aerodynamic data base and the computer simulation were revised accordingly in 1996. Since the error affected some of the lateral-directional aerodynamic data only it was fortunate that it had no influence on the aerodynamic trim model on which nearly all of the foregoing work had been based. This report summarises some stability and control investigations undertaken using models derived from the revised computer

simulation. All investigations were made for a neutrally buoyant airship. Three aspects of stability and control were studied in the limited time available.

(i) Since the aerodynamic data base had changed, the response to aerodynamic controls was revisited to confirm that the basic control characteristics were unchanged. Since most of the earlier work had concentrated on the higher speed end of the flight envelope the emphasis here is on the lower speeds in order to extend the understanding.

(ii) One of the main problems faced by the airship is a lack of control at low speed due to the poor performance of the aerodynamic controls. Thrust vectoring provides a useful means for control at very low speed and this was investigated as a part of the study.

(iii) Previous work by Crawford[2] on flying and handling qualities investigated the role of various aerodynamic derivatives in determining the dynamic characteristics of the airship. This work was based, in part, on an unpublished analysis by Lipscombe[3]. This work was also revisited, the analysis by Lipscombe was revised to more accurately reflect the characteristics of the aerodynamic model and the findings are included in this report.

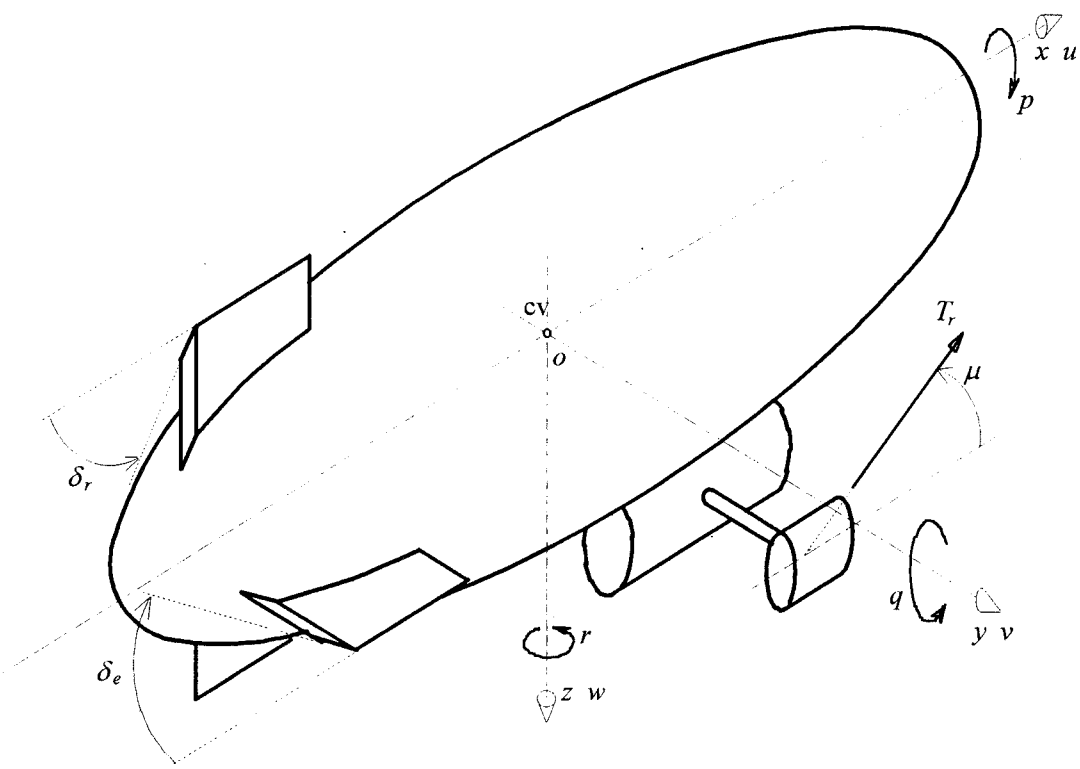

Fig.1 Body axis system in airship

2. Response to controls

2.1 The ACSL simulation

A comprehensive non-linear computer simulation model of the non-rigid airship was written by Gomes[1] in the *Advanced Continuous Simulation Language* (ACSL)[4]. Whenever the simulation is run, the initial conditions comprising speed, weight, thrust and buoyancy are specified. Firstly, the airship model is trimmed by the simultaneous adjustment of pitch attitude and the displacement air distribution in the ballonets. Once trim is achieved, the simulated manoeuvre may be initiated by displacement of the appropriate controls. For the present exercise, the controls comprised equivalent elevator δ_e, equivalent rudder δ_r, left and right engine thrust, T_l and T_r respectively, and thrust vector angle μ. For the purpose of modelling, a body axis system is fixed in the airship with its origin at the centre of volume as indicated in Fig.1. Also shown are the principal motion variables, linear and angular velocities, together with the control variables assumed for the present study. Output from the simulation comprises all, or any, of the control and motion variables as functions of time for the simulated response time.

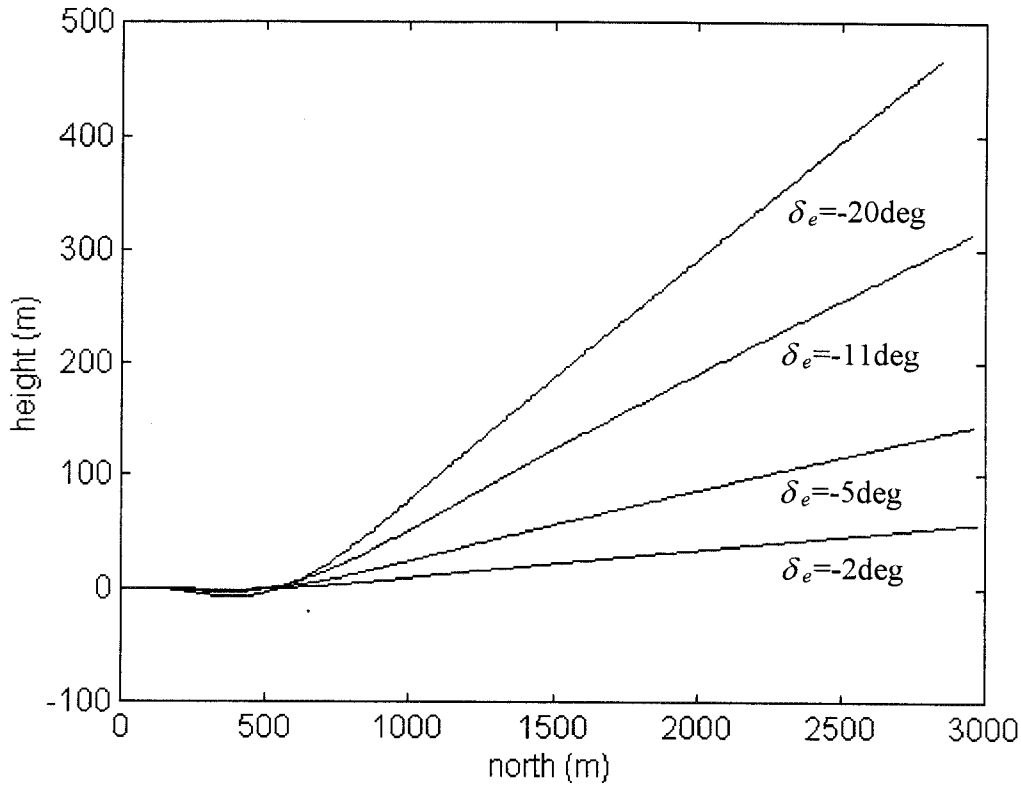

Fig.2 Flight path response to elevator step inputs at an initial speed of 25 m/s

2.2 Longitudinal responses to an elevator type input

With reference to Fig.1 it is clear that, for a given trimmed thrust, longitudinal manoeuvring may be effected by the equivalent elevator and, or, by varying the thrust vector angle of both engines symmetrically. Note that equivalent elevator implies the

symmetric displacement of the flap surfaces attached to both horizontal fins. In all simulated longitudinal manoeuvres the following response variables were recorded: height h, axial velocity u, normal velocity w, pitch rate q and pitch attitude θ.

2.2.1 Aerodynamic control

In order to establish an indication of the longitudinal control characteristics of the airship, response to elevator was measured at a typical cruising speed of 25 m/s. Flight path responses for elevator inputs of various magnitudes are shown in Fig.2. It is not surprising to see that the greater the elevator angle, the greater the rate of climb. It is also evident, especially at the larger elevator angles, that the down force on the tail surfaces causes the airship to sink initially until the hull develops sufficient lift to reverse the tendency and causes the airship to climb away. This *non-minimum phase* property is characteristic of most aeroplanes and is most significant when large pitch attitude changes are demanded. Time histories for the remaining motion variables are shown in Fig.3 for a -20° elevator step demand only. Clearly, the large change in pitch attitude causes a consequent reduction in speed due to the increase in drag.

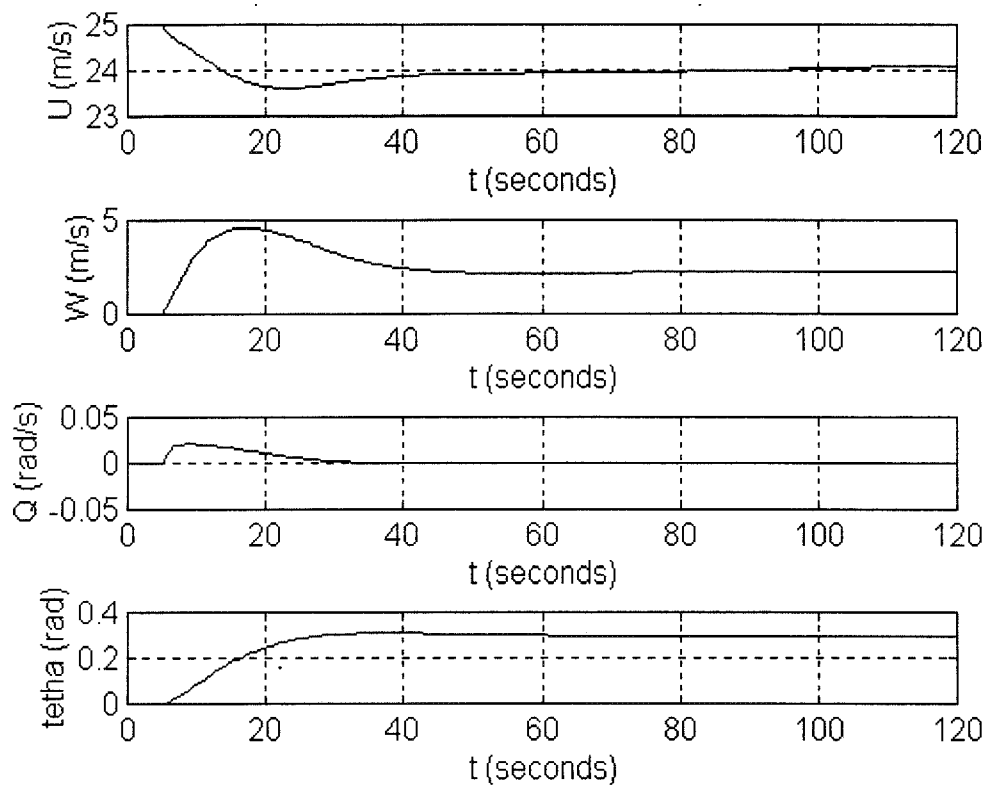

Fig.3 Longitudinal response to a -20° elevator step at a speed of 25 m/s

The sensitivity of the non-minimum phase characteristic to speed in the longitudinal response to elevator was examined further. Flight path response to a -11° elevator step is shown in Fig.4 for various speeds at the low speed end of the flight envelope. The sense of the elevator input is such as to demand pitch up to result in a climb. However, it is quite clear that at speeds below approximately 12 m/s, the hull is unable to develop sufficient lift to overcome the down load on the horizontal tail surfaces. The effect of longitudinal control at very low speeds is therefore reversed. This phenomenon is well-

known and it implies that the pilot has to reverse the input if he wants to climb at low speeds. Nevertheless, even if the pilot reverses the input, the amplitude of the response is negligible at the hover, or very small at very low speeds. This low speed control characteristics is one of the main disadvantages of the airship since it makes mooring and ground handling a difficult control problem which has still not been completely solved.

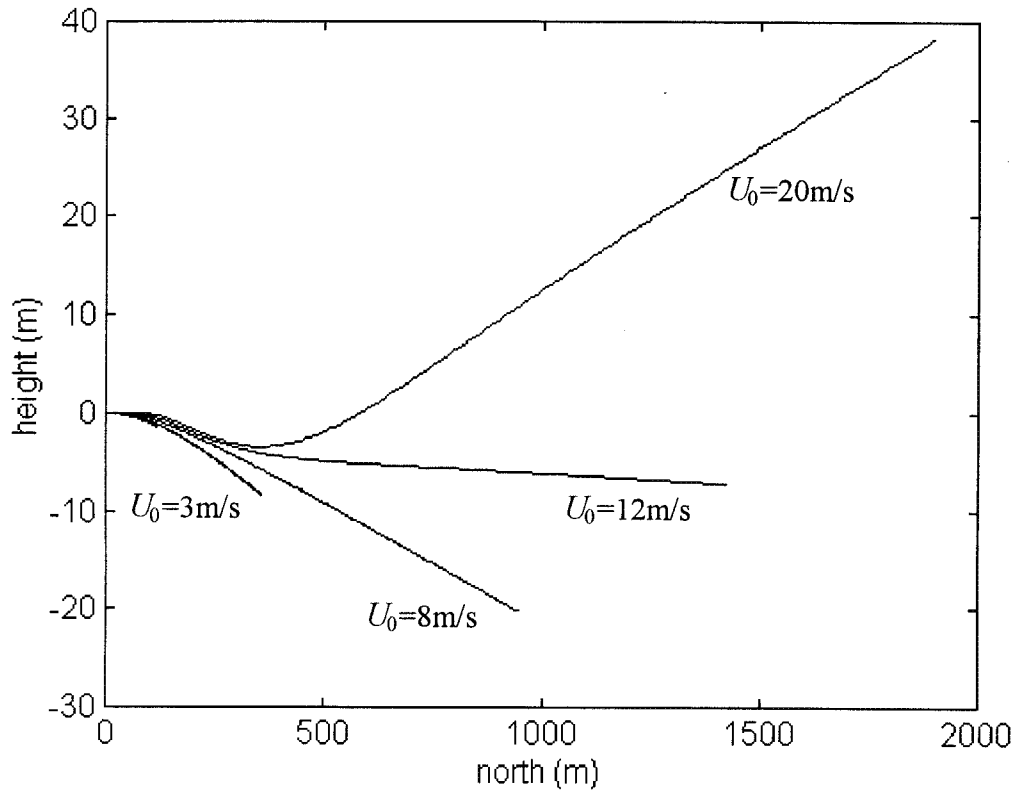

Fig.4. The sensitivity of longitudinal control to speed

2.2.2 Comparison between vectoring thrust and aerodynamic control

Two representative low speed situations which are difficult to manage were studied, the hover and the initial take-off manoeuvre. The hover is a particularly difficult control condition since the aerodynamic controls are essentially ineffective and thrust control is the only mechanism available to the pilot for short term control of the vehicle. Clearly, the control problem is compounded in the presence of atmospheric disturbances. The take-off manoeuvre, especially the part which is below the control reversal speed, also poses an interesting control problem for the pilot. It is usual practice to use thrust vectoring to assist the take-off manoeuvre.

To simulate a thrust control input, a symmetric thrust vector angle step μ and a small symmetric step increase in thrust were demanded simultaneously. Consequently, the small change in thrust magnitude resulted in a small change in the trimmed speed. In order to achieve a meaningful comparison of the responses to the vectoring thrust with the response to aerodynamic control, the small step in thrust magnitude was also applied simultaneously with the aerodynamic control input.

Since it is not possible to achieve a true zero speed hover with the simulation model, the hover was modelled with a very small axial velocity of 0.1 m/s. Response to the control input was recorded for 120 seconds and the small step in thrust magnitude caused the speed to increase to 0.6 m/s at the end of this observation period. The results of this experiment, limited to flight path responses only, are shown in Fig.5.

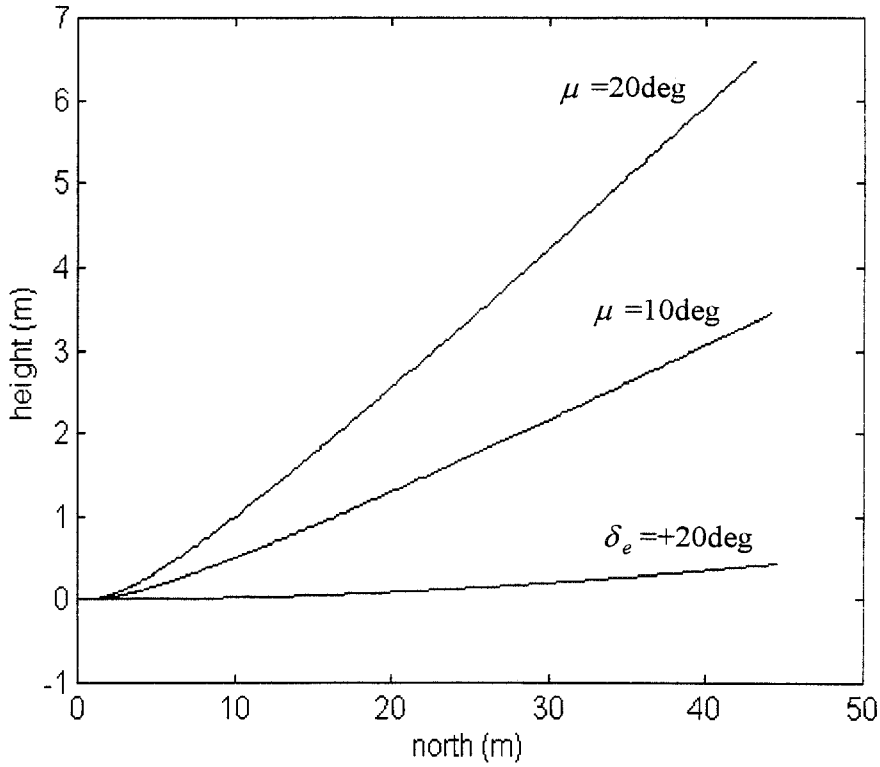

Fig.5 Comparison between vectored thrust and aerodynamic control at hover

Clearly, thrust vectoring provides a much more effective means for control at very low speed. Note that the maximum aerodynamic control input is applied in the pitch down sense (positive) in order to demand climb. Its effectiveness is very poor, as might be expected, since the airship climbs less than 0.5 m in 120 seconds. The responses to thrust vectoring are, in comparison, rather better. Besides, it is possible to utilise a large thrust angle to achieve greater control effectiveness.

The take-off simulation flight path responses are shown in Fig.6. The initial condition for the simulation was hover at ground level, and as before, the hover was approximated by an axial speed of 0.1 m/s. The thrust magnitude step was chosen to give a climb out speed of 11 m/s at the end of the simulation run time of 120 seconds.

Once again, it is clearly evident that thrust vectoring provides a more effect control mechanism for initiating the take-off manoeuvre, especially for thrust vector angles greater than 10°. Again, the aerodynamic control input is reversed in order to initiate a climb response. However, once the speed has reached 12 m/s, it was found that the aerodynamic control is sufficiently effective to be the main source of longitudinal control.

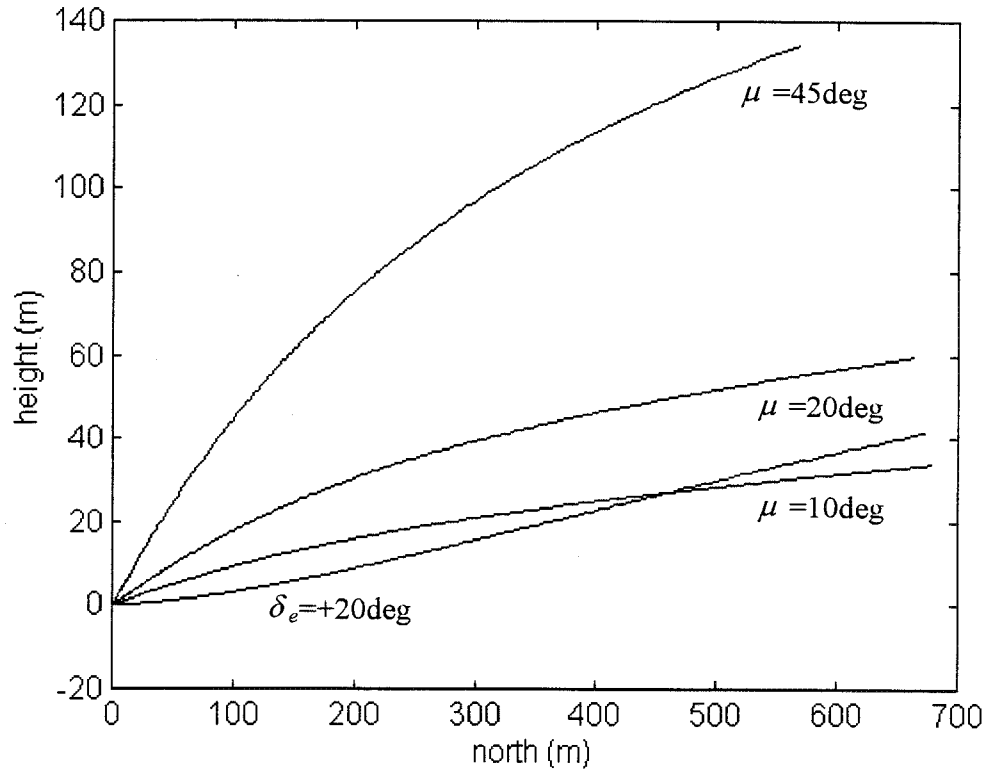

Fig.6 Comparison of thrust vectoring and aerodynamic control at take-off

2.2.3 Observations

Thrust vectoring provides an effective alternative to the aerodynamic elevator control for the low speed range. This low speed range, below approximately 12 m/s, can be described as the range where, in response to a control input, the dominant lift is not provided by the hull but by the fin itself. For all longitudinal operations in this low speed range, thrust vectoring could be used as the primary means of control. This implies that when an airship is fitted with thrust vectoring controls, the dimensions of the elevators could be reduced since they would only be required for control at high speeds

2.3 Lateral-directional responses to a rudder type input

With reference to Fig. 1, lateral-directional manoeuvring may be effected by the equivalent rudder δ_r and, or, by differential variation of the magnitude of the thrust of the right and left engine, T_r and T_l respectively. Note that equivalent rudder implies the symmetric displacement of the flap surfaces attached to both vertical fins. The airship does not have an equivalent aileron and therefore direct control in roll is not possible. Direct roll control is not necessary since the main source of lift is buoyancy and the lift vector is always directed upwards. In all simulated lateral-directional manoeuvres the following response variables were recorded, lateral displacement referred to earth axes, lateral velocity v, roll rate p, yaw rate r and roll attitude ϕ.

2.3.1 Aerodynamic control

To establish the aerodynamic effectiveness of the equivalent rudder control, turning response at the typical cruise speed of 25 m/s was evaluated for step inputs of various magnitudes as shown on Fig.7. As might be expected, the radius of turn is reduced as the rudder angle is increased. Note that no non-minimum phase effect is apparent in directional control. Clearly, the rudder is an effective means for directional control at the speed in question.

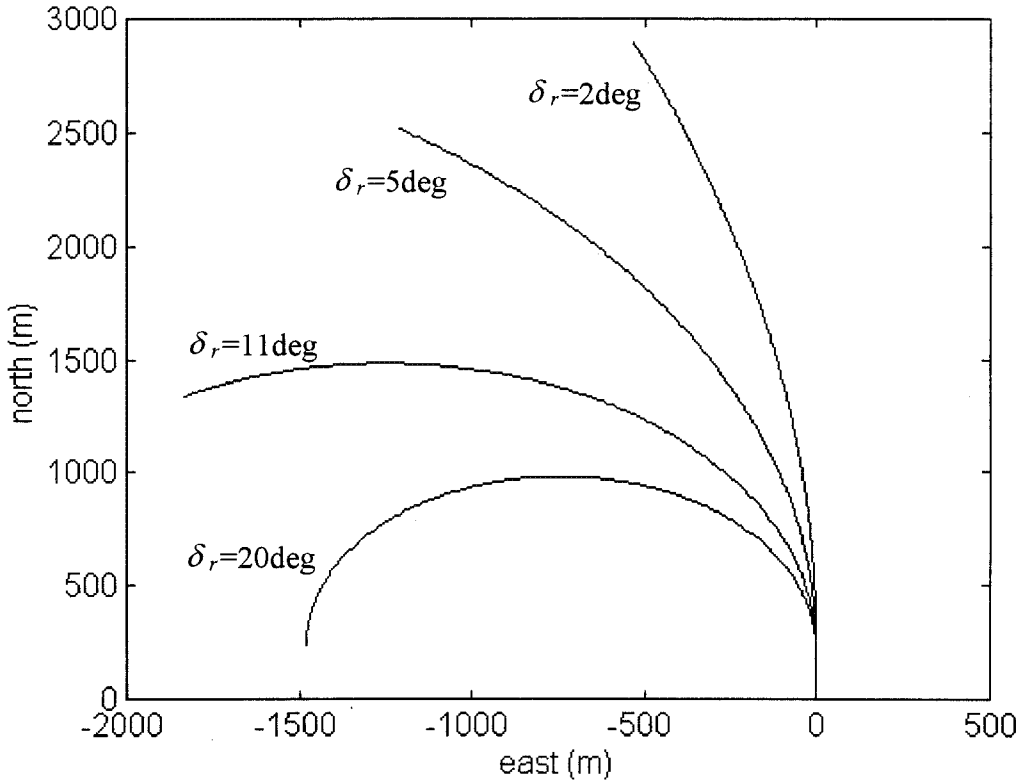

Fig.7 Track response to a rudder step input at an initial speed of 25 m/s

Corresponding time histories for the remaining motion variables in response to a rudder step input of -20° are shown in Fig.8. The oscillation which is clearly visible in the roll rate response is the oscillatory roll mode which is lightly damped at this flight condition.

In order to establish if there is also a reversal speed in directional control, the response to rudder was examined further. Track response to a -11° rudder step input is shown in Fig.9 for various speeds at the low speed end of the flight envelope. It is clearly, evident that the turning performance is almost independent of speed, the radius of turn being nearly constant. It is also clear that normal aerodynamic control may be maintained at a speed as low as 3 m/s, the lowest recorded. It would therefore appear that directional control reversal does not occur at low speed.

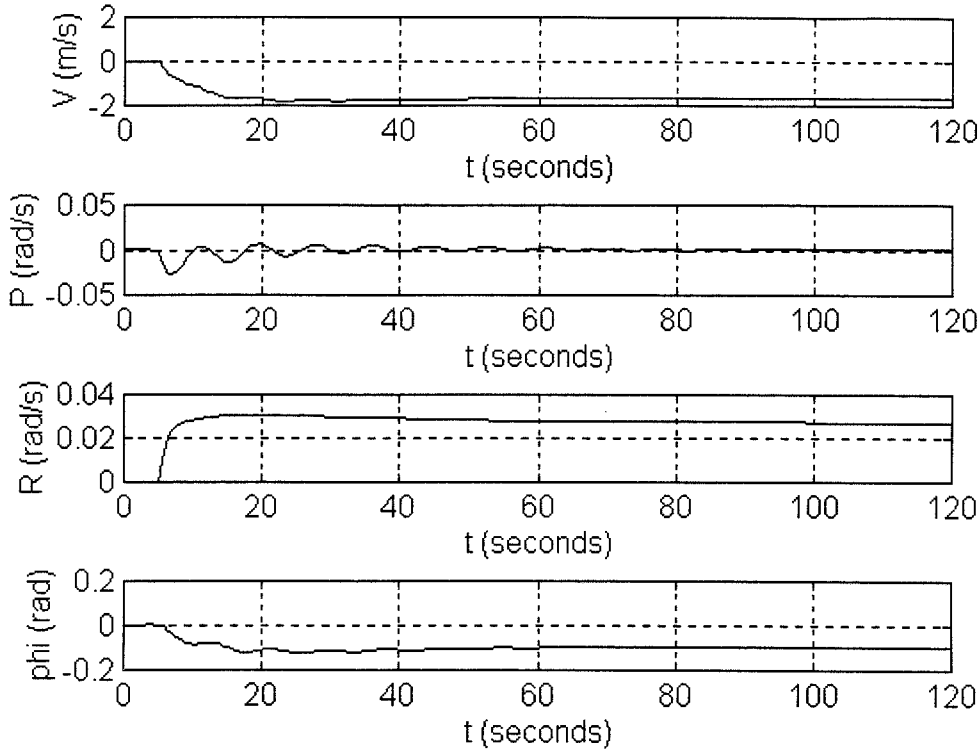

Fig.8 Lateral-directional response to a -20° rudder step at a speed of 25 m/s

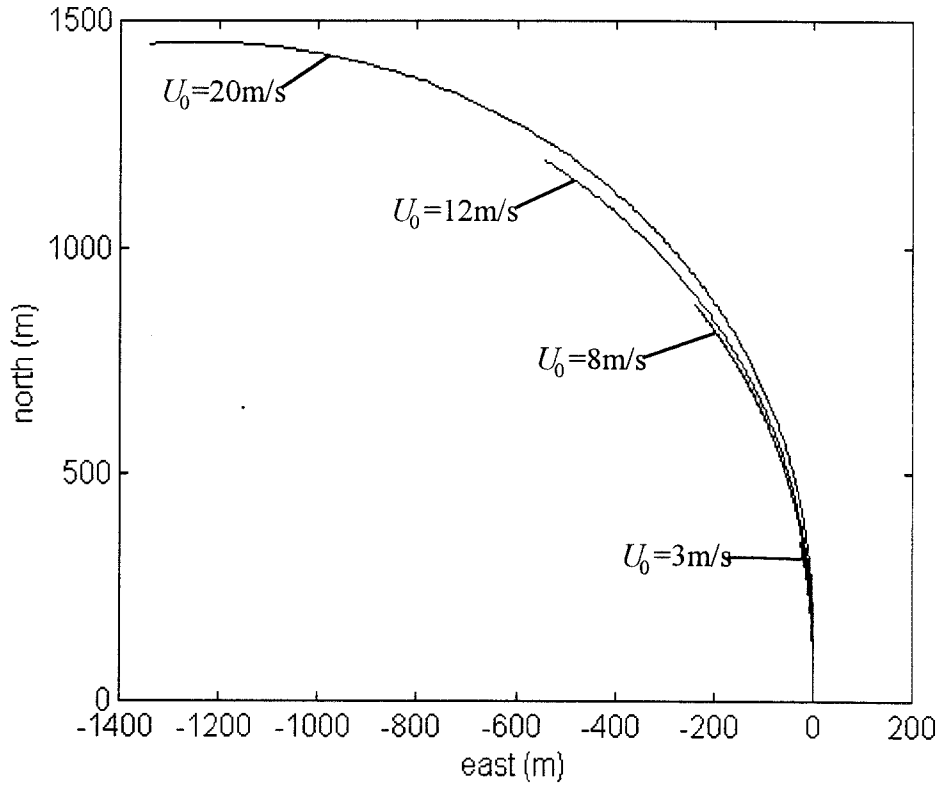

Fig.9 The sensitivity of directional control to speed

2.3.2 Comparison between differential thrust and aerodynamic directional control

Differential thrust and rudder were compared for directional control in a situation representative of a landing approach. The simulation reproduces a left turn toward the mooring mast at an initial speed of 2 m/s. The simulation run time was limited to 25 seconds to establish what level of performance can be achieved in a relatively short time. The ground track responses are compared in Fig.10.

Thrust control was simulated by simultaneously increasing the thrust on the right engine by a fixed amount and by reducing the thrust on the left engine by the same amount to induce a turn to the left. In the first instance, the thrust increment was $\pm 20T$ and in the second instance the thrust increment was $\pm 40T$ where T was the initial trim value of thrust. To simulate engine response time the thrust increment was applied as a short ramp function rather than a step function. Even in the second case, the forty fold increase in thrust was still representative of less than a quarter of the maximum power available, which is 2070 bhp. Thrust control was compared with the maximum equivalent rudder displacement of 20° as indicated in Fig.10.

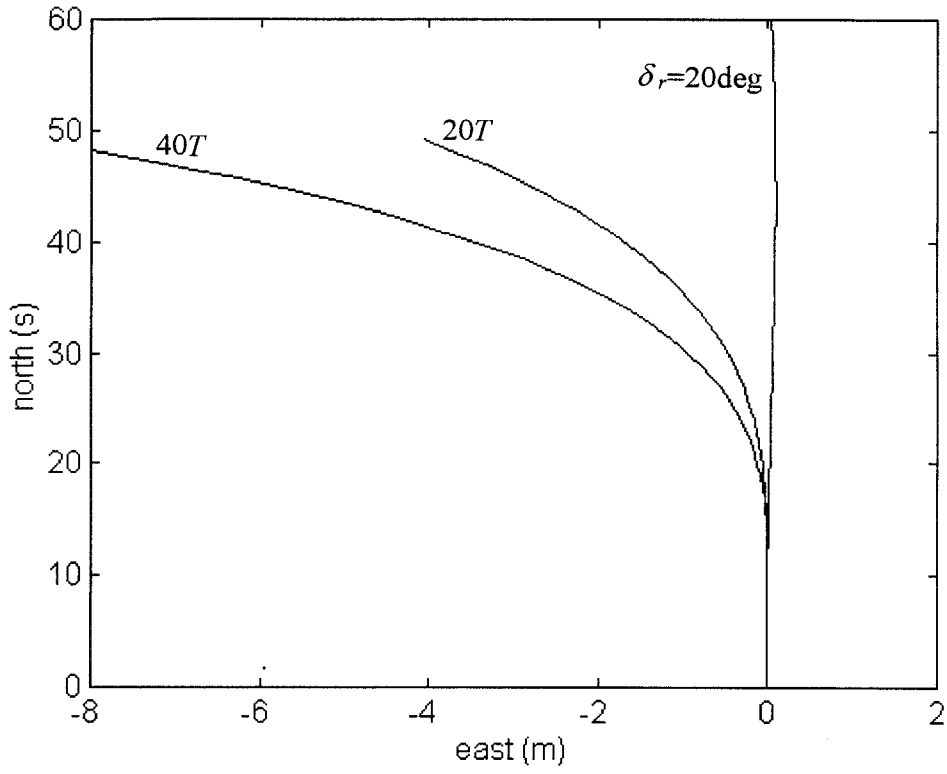

Fig.10 Comparison between differential thrust and aerodynamic control in a landing approach.

Fig.10 indicates that, as might be expected, differential thrust is far more effective than aerodynamic control. The large scale of the response plot reveals that there is a small non-minimum phase effect with aerodynamic control at this very low speed. Thus, for the first 25 seconds after control input, any lateral displacement due to rudder is almost impossible. This emphasises the importance of differential thrust for lateral-directional manoeuvring during mooring and ground handling.

Corresponding time histories for the remaining motion variables in response to a differential thrust input are shown in Fig.11. Again, the oscillation which is clearly visible in the roll rate response, although its amplitude is very small indeed, is the oscillatory roll mode which is essentially a lateral pendulum mode at this lightly damped low speed flight condition.

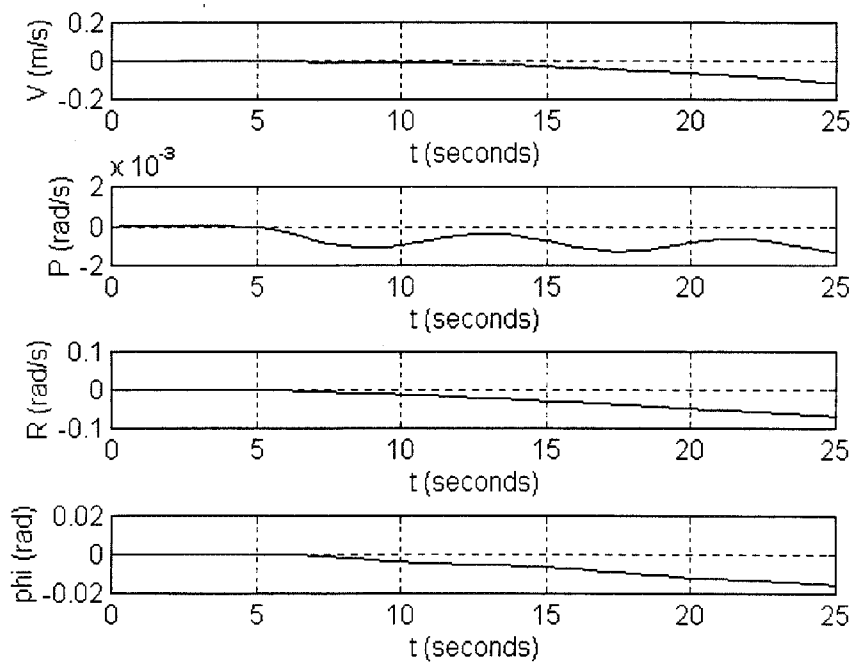

Fig.11 Lateral-directional response to a differential thrust input

2.3.3 Observations

Differential thrust control provides an effective alternative to rudder control for manoeuvring at very low speeds. Although control reversal is barely perceptible in response to rudder at the very lowest speeds, the rudder is not an effective means for control at low speeds. Thus differential thrust is the only useful means for directional control of the airship during a landing approach, and when rapid response is required at low speed.

3. Linear analysis

3.1 State model

To facilitate mathematical analysis of airship dynamics it is first necessary to derive a linear de-coupled model from the non-linear system of equations of motion described in Appendix 1. A full description of the derivation of the linear equations of motion is given in Cook[5]. However, in this work a very powerful feature of ACSL was used to obtain numerical values for the linear state model at a predetermined operating condition.. The ANALYSE command in ACSL enables the state and input matrices, from the linear state equation, to be extracted for a given set of state variables at a defined operating point. In this work those matrices were obtained one second into the response following an elevator or rudder step input. The de-coupling of the longitudinal handling from the lateral-directional handling has long been established for the airship. In the Zeppelins, for example, there were two control wheels, one for the rudders and one for the elevators, each being operated by its own crew member.

With reference to Cook[5], the general state equation may be written in the standard form,

$$\dot{\mathbf{x}} = \mathbf{A}\mathbf{x} + \mathbf{B}\mathbf{u} \tag{1}$$

where, **A** is the state matrix, **B** is the input matrix, **x** is the state vector and **u** is the input vector.

Thus, the longitudinal state equation may be written,

$$\begin{bmatrix} \dot{u} \\ \dot{w} \\ \dot{q} \\ \dot{\theta} \end{bmatrix} = \begin{bmatrix} x_u & x_w & x_q & x_\theta \\ z_u & z_w & z_q & z_\theta \\ m_u & m_w & m_q & m_\theta \\ 0 & 0 & 1 & 0 \end{bmatrix} \begin{bmatrix} u \\ w \\ q \\ \theta \end{bmatrix} + \begin{bmatrix} x_{\delta_c} & x_{\delta_t} \\ z_{\delta_e} & 0 \\ m_{\delta_e} & m_{\delta_t} \\ 0 & 0 \end{bmatrix} \begin{bmatrix} \delta_e \\ \delta_t \end{bmatrix} \tag{2}$$

and the lateral-directional state equation may be written,

$$\begin{bmatrix} \dot{v} \\ \dot{p} \\ \dot{r} \\ \dot{\phi} \end{bmatrix} = \begin{bmatrix} y_v & y_p & y_r & y_\phi \\ l_v & l_p & l_r & l_\phi \\ n_v & n_p & n_r & n_\phi \\ 0 & 1 & 0 & 0 \end{bmatrix} \begin{bmatrix} v \\ p \\ r \\ \phi \end{bmatrix} + \begin{bmatrix} y_{\delta_r} \\ 0 \\ n_{\delta_r} \\ 0 \end{bmatrix} \delta_r \tag{3}$$

The longitudinal and lateral-directional state equations were solved, with the aid of MATLAB[6], to obtain the transfer function matrices $\mathbf{G}(s)$ where,

$$\mathbf{G}(s) = \frac{[s\mathbf{I} - \mathbf{A}]^T \mathbf{B}\mathbf{u}}{\det[\mathbf{sI} - \mathbf{A}]} \equiv \frac{\mathbf{N}(s)}{\Delta(s)} \tag{4}$$

$\mathbf{N}(s)$ denotes the numerator matrices, the elements of which are the numerator polynomials in the Laplace operator s, and $\Delta(s)$ denotes the characteristic polynomial, the poles of which determine the stability characteristics of the airship .

All the response transfer functions obtained by this means are presented in Appendix 3.

3.2 Comparison of the non-linear model with the linear model

The comparisons were made at two different flight speeds, 8 m/s and 25 m/s respectively, and for an elevator or rudder step input of -11°.

The longitudinal motion comparisons are shown, for the two speeds, in Fig.12 and Fig.13 respectively. In each of the following response plots, the solid black trace is the non-linear response as given by ACSL and the dotted trace is the linear response as given by MATLAB. It is evident that the match between the two models is really good except for the surge speed at 25 m/s. This is because the surge speed depends on coupled terms which are not included in the linear MATLAB model. Nevertheless, the difference in speed is sufficiently small that the longitudinal linear state model can be considered to give an acceptable representation of the airship dynamics for short to medium term periods of observation.

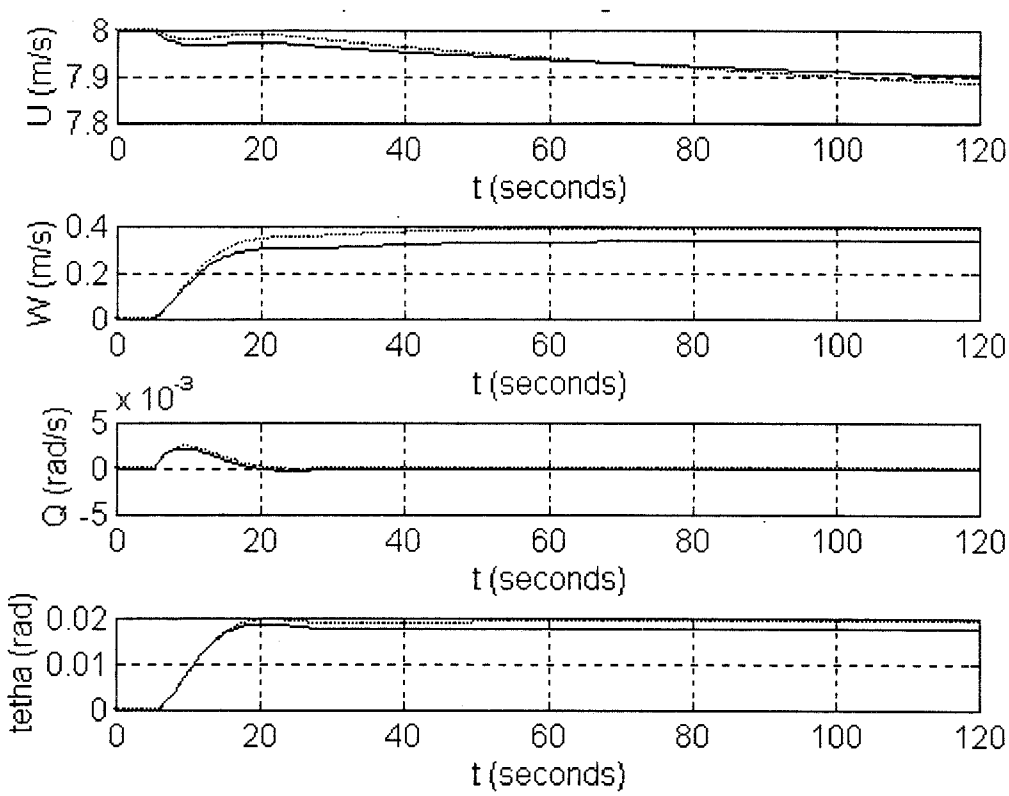

Fig.12 Response to a -11° elevator step at U_0=8 m/s

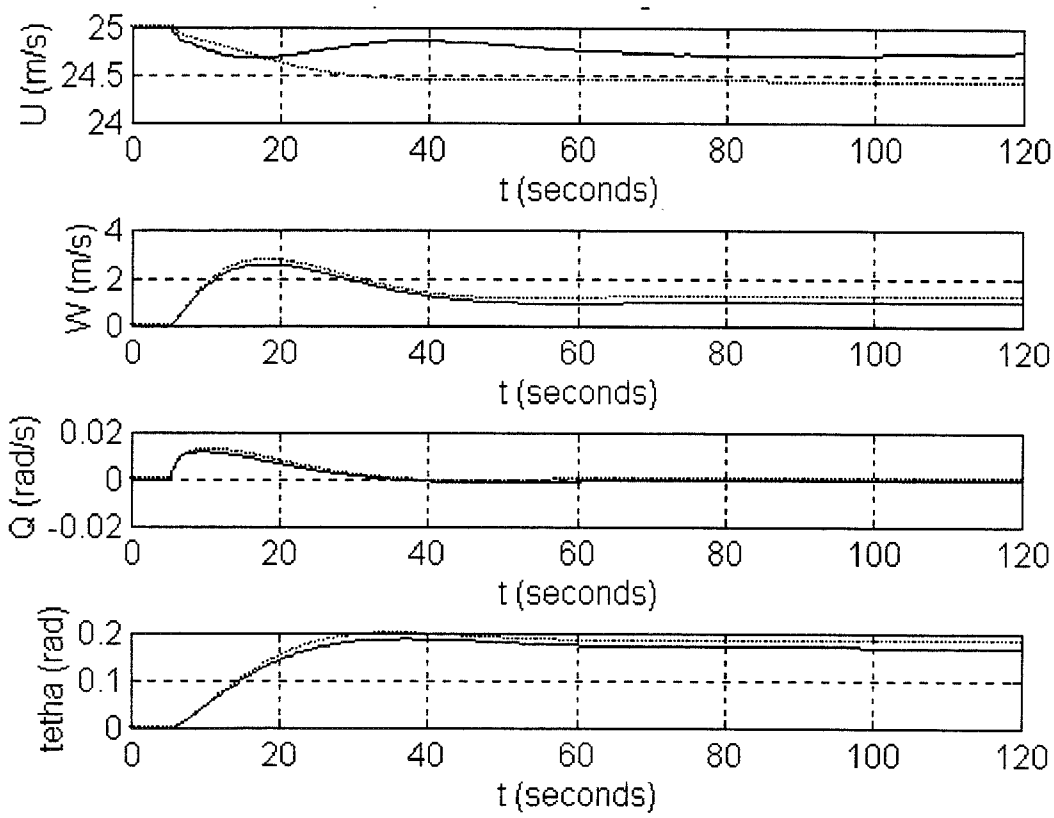

Fig.13 Response to a -11° elevator step at U_0=25 m/s

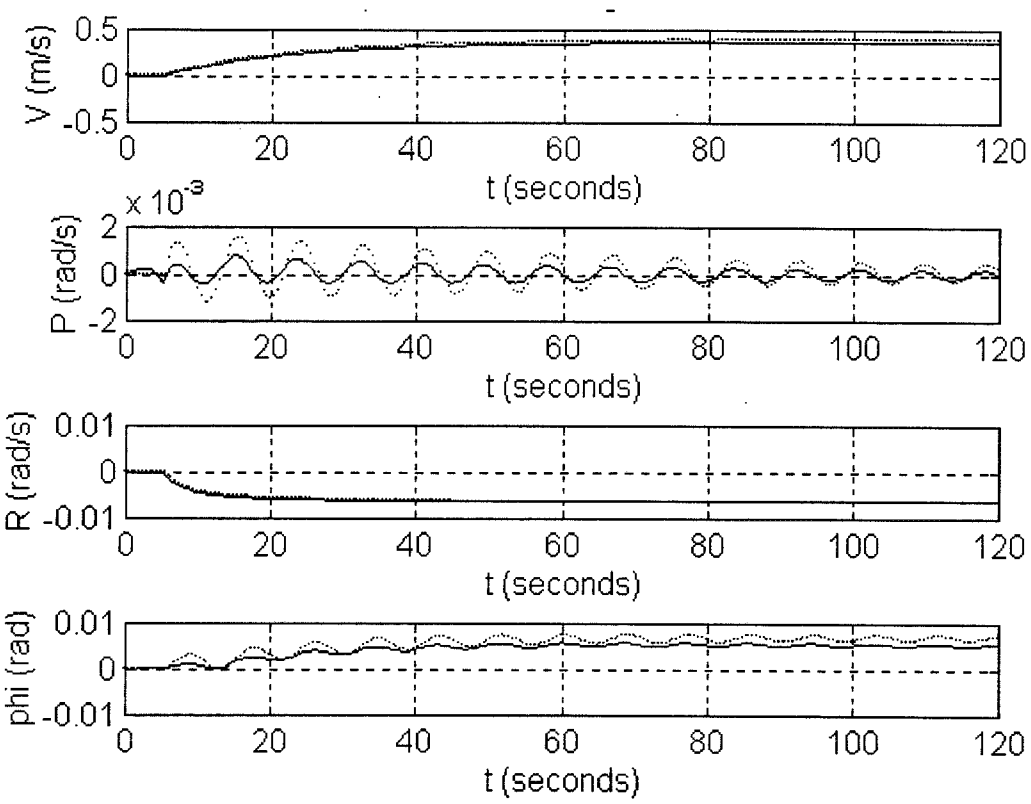

Fig.14 Response to a -11° rudder step at U_0=8 m/s

The lateral-directional motion comparisons are shown, for the two speeds, in Fig.14 and Fig.15 respectively. As before, in each of the response plots, the solid black trace is the non-linear response as given by ACSL and the dotted trace is the linear response as given by MATLAB. The comparison of the two models shows that there is a small difference in roll rate, and therefore in roll attitude as well, which increases with speed. However, the fundamental shapes of the responses are very similar. Clearly, the dynamic coupling omitted in the linearised lateral-directional model is rather more significant. The differences are considered to be sufficiently small that the lateral-directional linear state model can be considered to give an acceptable representation of the airship dynamics for short to medium term periods of observation.

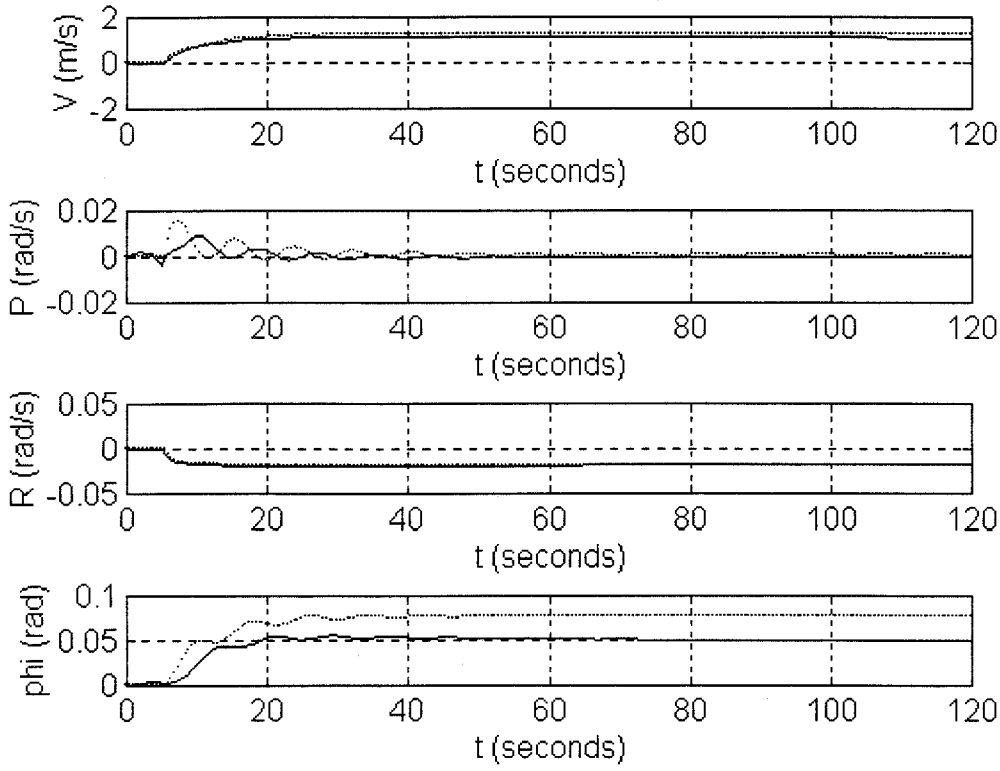

Fig.15 Response to a -11° rudder step at U_0=25 m/s

3.3 Stability modes analysis

3.3.1 The longitudinal modes

Lipscombe[3] undertook an algebraic analysis of the equations of motion based on approximations dependent upon typical relative magnitudes of the matrix coefficients. The results of this analysis enabled the longitudinal stability modes characteristics to be described in terms of approximate algebraic expressions comprising the matrix coefficients. Lipscombe's original work has been reviewed and an addition has been made to this work in order to establish analytically what Lipscombe demonstrated numerically. The analyses are set out in Appendix 2.

Having established approximate models to described the longitudinal stability modes, it was then considered necessary to test the validity of the models. This was done by

measuring the modes characteristics at various speeds using the full non-linear simulation model and comparing the modes characteristics with the approximations. The numerical values of the coefficients of the **A** and **B** matrices comprising the linear model are given in Appendix 3, together with the transfer function poles, zeros and gains obtained in the solution of the equations of motion. It should be remembered that the linear models set out in Appendix 3 were obtained from the non-linear simulation model by linearising about a chosen speed.

Surge mode

The longitudinal surge mode is characterised as a lag in axial speed response and, as shown by the analysis in Appendix 2, is dominated by the derivative x_u. In Fig.16 the value of the derivative x_u is plotted as a function of forward speed and the plot is overlaid with a number of points representing the actual value of the surge mode pole at various speeds. Both the values of the derivative x_u and the surge mode pole were obtained from the models given in Appendix 3. It is clear that the comparison is very good implying that the surge mode pole is well represented by $(s - x_u)$.

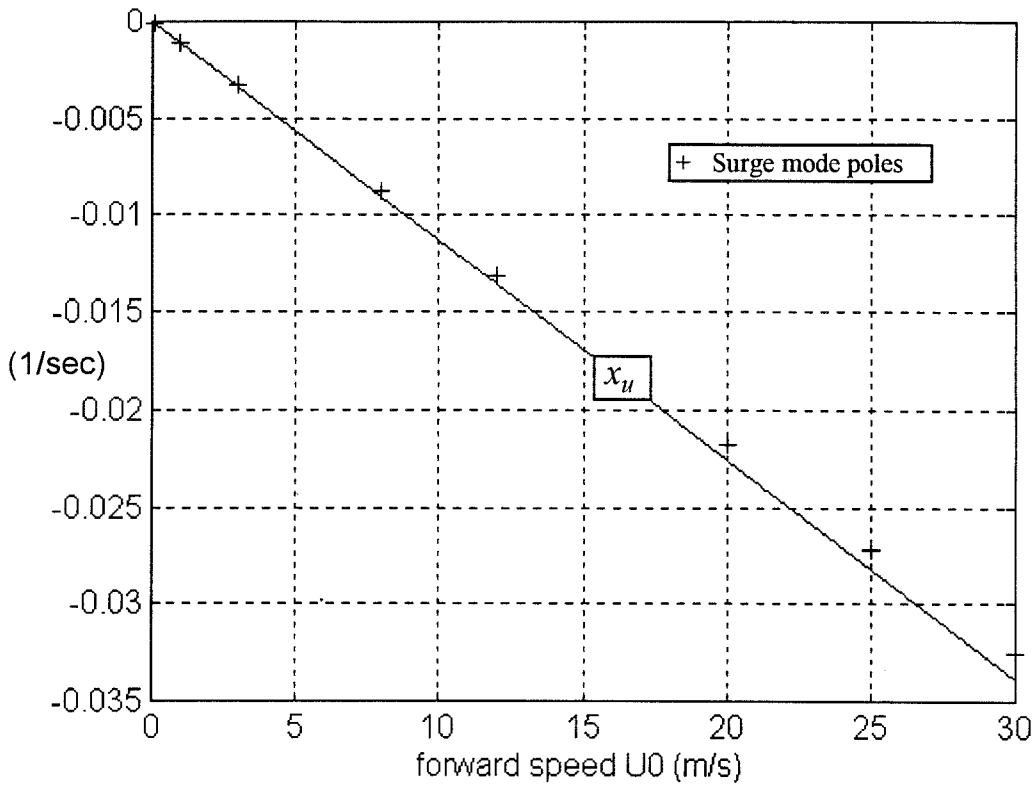

Fig.16 Surge mode characteristic

Heave and Pitch subsidence mode

As Lipscombe demonstrated, at low speed the heave mode is characterised approximately by z_w and at high speed it becomes a pitch mode characterised approximately by m_q. This characteristic is also demonstrated in the response to an elevator step input at different speeds. At low speeds, the response is poor whereas, at high speed the response is good. The transition from a heave subsidence characteristic to a pitch subsidence characteristic occurs at the *transition speed* which, it may be observed from Fig.17, is nominally around 12 m/sec. Below this speed, the pilot will experience longitudinal elevator control reversal because the hull is unable to generate enough lift to climb, which is in accordance with the findings in paragraph 2.2.1. The values for the derivatives z_w and m_q are shown plotted as functions of speed in Fig.17. Super-imposed on these plots is the mode pole, and at low speeds the pole aligns closely with z_w whereas, at high speed the pole aligns closely with m_q. The values of the derivatives z_w and m_q and the heave/pitch mode pole were obtained from the models given in Appendix 3. It is clear that the comparison is very good implying that the low speed heave mode pole is well represented by $(s - z_w)$, and the higher speed pitch mode pole is well represented by $(s - m_q)$.

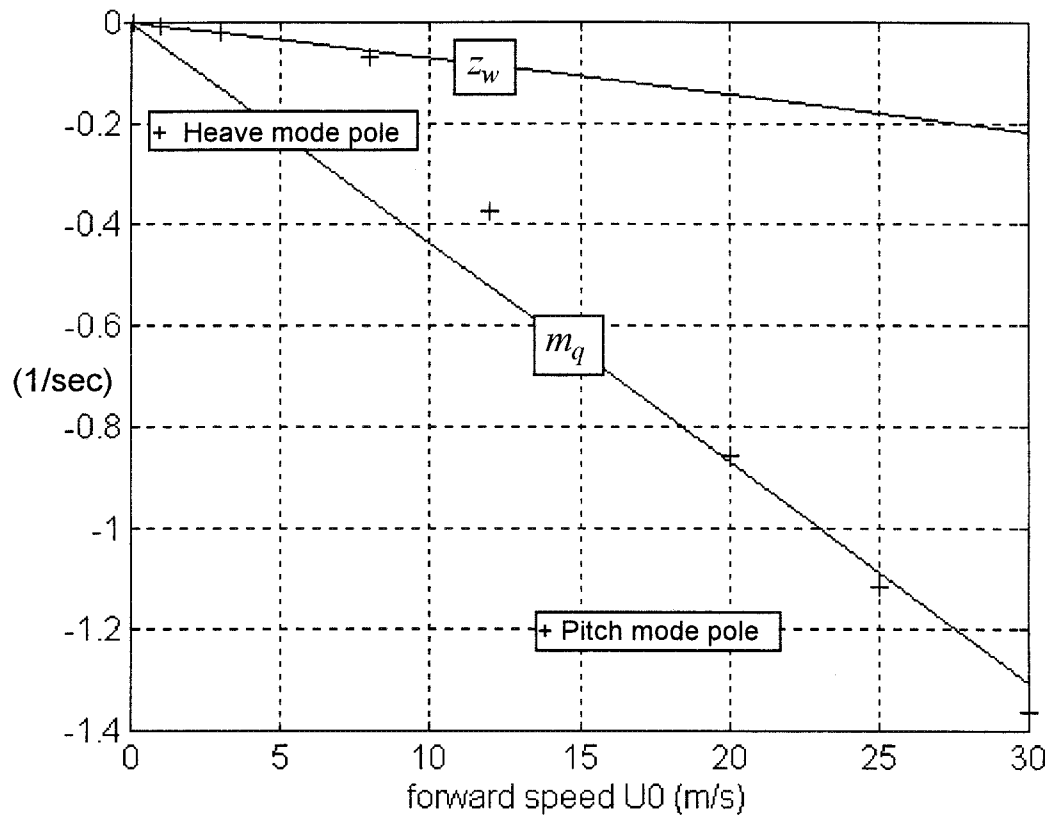

Fig.17 Heave and pitch subsidence mode characteristic.

Pendulum mode

At low speeds the pendulum mode is characterised approximately by $\left(s^2 - m_q s - m_\theta\right)$. At higher speeds, the pendulum mode is modified by an incidence-pitch angle interaction and is characterised approximately by $\left(s^2 - z_w s - \frac{m_\theta z_w}{m_q}\right)$. The variation of frequency and damping ratio of the mode is shown in Fig.18.

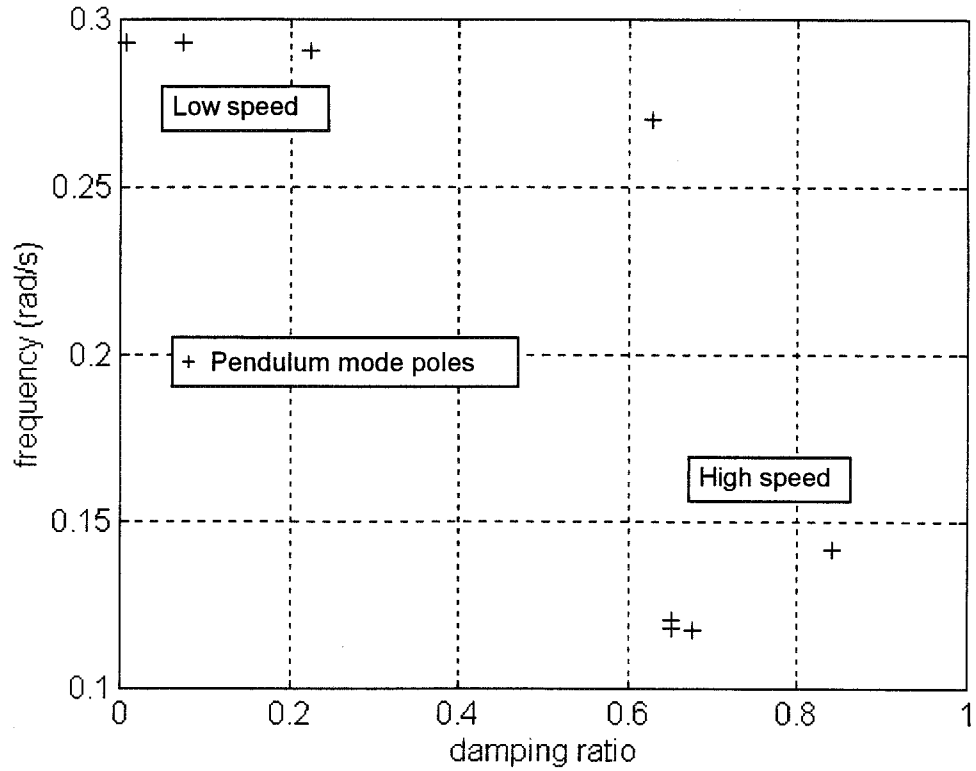

Fig.18 Longitudinal pendulum mode

3.3.2 The lateral-directional modes

As the corrections to the aerodynamic data base mainly influence the lateral-directional handling, the original assumptions made by Lipscombe[3] were revised as described in Appendix 2.

Sideslip subsidence mode

Fig.19 shows the plot of the approximate sideslip subsidence pole as given by the expression, $\left(y_v - l_v y_\phi / l_\phi\right)$. Superimposed on the plot are the mode poles as given for the various speeds in Appendix 3. Clearly, the approximation is good. At low speeds, the pole is near zero which implies that, since the mode is nearly neutrally stable, the pilot has very poor control of sideslip at those speeds, which supports the observations made in paragraph 2.3.

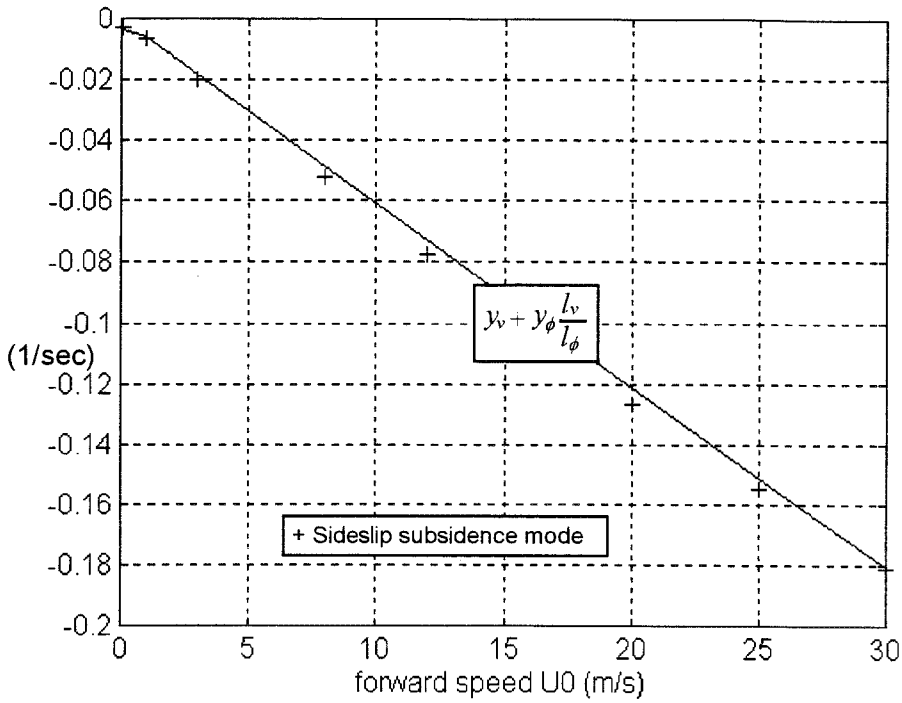

Fig.19 Sideslip subsidence mode characteristic

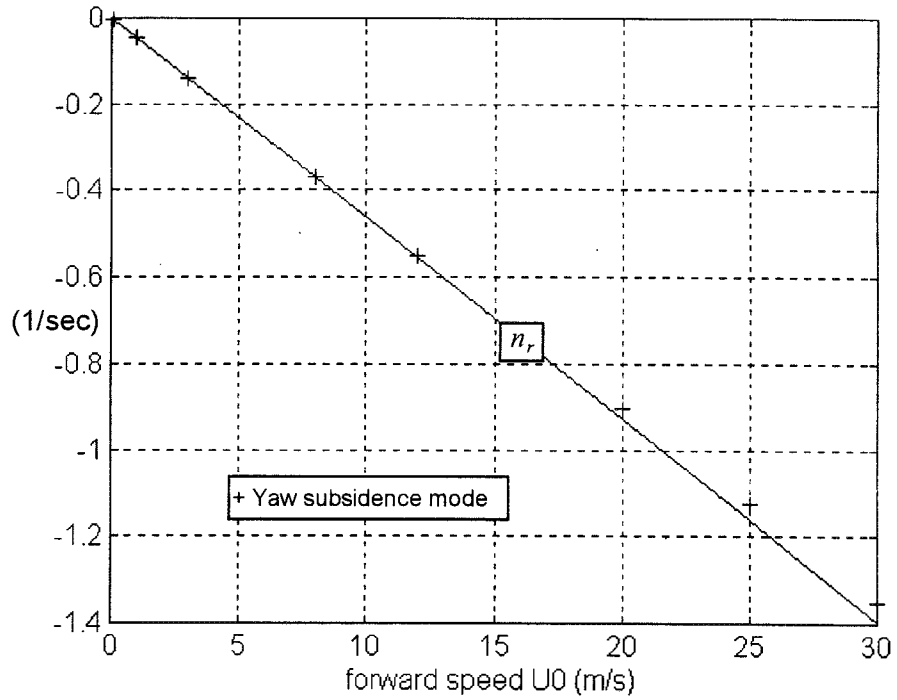

Fig.20 Yaw subsidence mode characteristic

Yaw subsidence mode

Fig.20 shows plot of the approximate yaw subsidence pole as given by the yaw damping derivative n_r. as before, superimposed on the plot are the poles as given for the various speeds in Appendix 3. Again, the approximation is good. At slow speeds,

the pole is near zero which implies that, since the mode is nearly neutrally stable, the pilot has very poor control of yaw at those speeds, which corresponds with the observations made in paragraph 2.3.

Oscillatory roll mode

The oscillatory roll mode is characterised approximately by,

$$\left(s^2 - \left(l_p + y_v - \frac{l_v y_\phi}{l_\phi}\right)s - l_\phi\right)$$

The variation of frequency and damping ratio of the mode is shown in Fig.21.

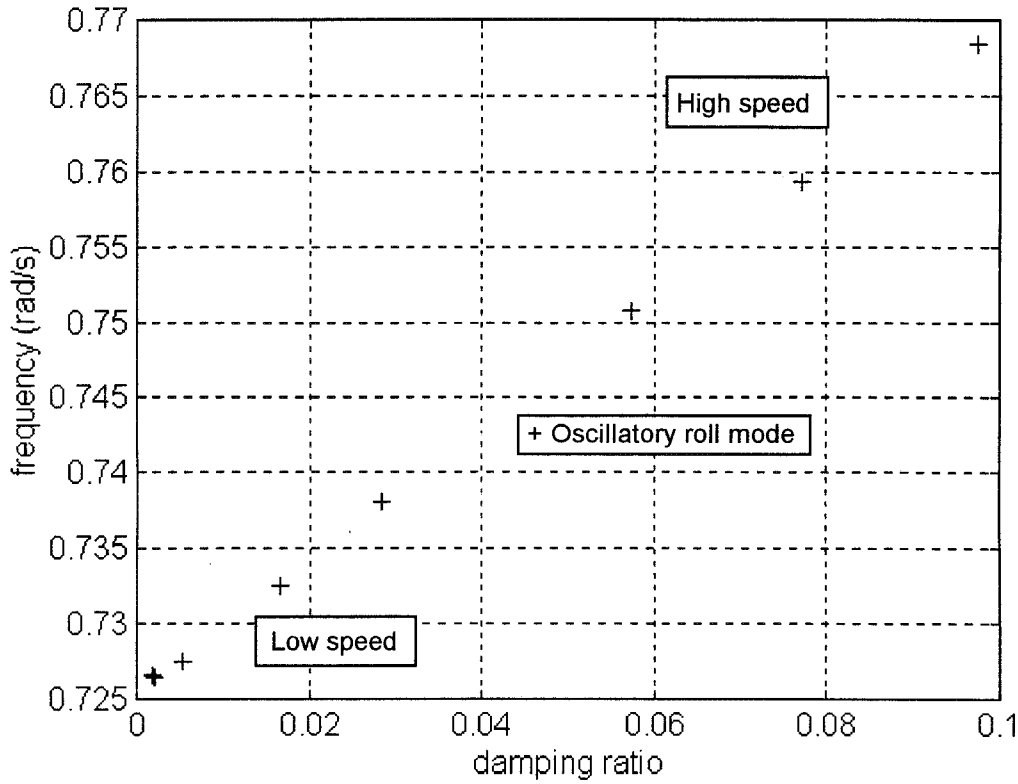

Fig.21 Oscillatory roll mode characteristic

4. Conclusions

- Longitudinal elevator control reversal occurs at speeds below approximately 12 m/s. At speeds below this transition speed, thrust vector control is more effective for longitudinal manoeuvring.

- There is no discernible control reversal in aerodynamic directional control at any speed. However, at speeds below approximately 3 m/s aerodynamic directional control becomes ineffective. Below this speed, differential thrust is more effective for lateral-directional control.

- The short term response of the linear longitudinal model matches the response of the non-linear simulation model well. The linear model is therefore considered adequate for short term stability and control analysis.

- The short term response of the linear lateral-directional model matches the response of the non-linear simulation model reasonably well. Therefore, with care, the linear model is considered satisfactory for short term stability and control analysis.

- All of the stability modes are stable at all of the speeds for which they were analysed.

- All of the stability modes therefore describe convergent characteristics. However, at low speeds all of the poles are near to zero, implying near neutral stability and very slow convergence. Therefore, pilot control of the airship is very poor at low speeds as demonstrated in the earlier part of the study.

- By making appropriate assumptions about the nature of airship motion, approximate models of the stability mode poles were found by analysing the linear equations of motion. These models were found to give very good estimates for the actual stability mode poles.

- The approximate low speed longitudinal stability mode poles expressed as functions of concise derivatives were established,

Speed subsidence, or surge mode	$(s - x_u)$
Heave subsidence mode,	$(s - z_w)$
Longitudinal pendulum mode	$(s^2 - m_q s - m_\theta)$

- The approximate high speed longitudinal stability mode poles expressed as functions of concise derivatives were established,

Speed subsidence, or surge mode	$(s - x_u)$
Pitch subsidence mode	$(s - m_q)$
Longitudinal pendulum mode	$\left(s^2 - z_w s - \frac{m_\theta z_w}{m_q}\right)$

- The approximate lateral-directional stability mode poles, for all speeds, expressed as functions of concise derivatives were established,

Yaw subsidence mode	$(s - n_r)$
Sideslip subsidence mode	$\left(s + y_v - \frac{l_v y_\phi}{l_\phi}\right)$
Oscillatory roll mode	$\left(s^2 - \left(l_p + y_v - \frac{l_v y_\phi}{l_\phi}\right)s - l_\phi\right)$

References

[1] Gomes, S.B.V. *An Investigation of the Flight Dynamics of Airships with Application to the YEZ-2A*. College of Aeronautics PhD thesis, Cranfield Institute of Technology. 1990

[2] Crawford, J.P. *Research into the Flying and Handling Qualities of an Airship*. College of Aeronautics MSc thesis, Cranfield Institute of Technology. 1993

[3] Lipscombe, J.M. *Unpublished communication*. College of Aeronautics, Cranfield Institute of Technology. 1988

[4] *The Advanced Continuous Simulation Language (ACSL)*. Mitchell and Gauthier Associates, Concord, Massachusetts 01742-3096.

[5] Cook, M.V. *Stability and Control.* Chapter IV in **Airship Technology**. (Eds. Khoury, G.A. and Gillett, J.D.), Cambridge University Press. 1999

[6] *PC MATLAB*. The Mathworks Inc., Natick, Massachusetts 01760.

APPENDICES

Appendix 1: The equations of motion

The equations of motion of the airship have been set out variously by Gomes[1] and Cook[5]. The axis system used here is a body fixed system as shown in Fig.1, with the origin coincident with the centre of volume of the envelope. As is usual, a rigid body model is assumed and the oxz axes define a plane of symmetry. The governing state equation may be written,

$$\begin{bmatrix} m_x & 0 & 0 & 0 & ma_z & 0 \\ 0 & m_y & 0 & -ma_z & 0 & ma_x \\ 0 & 0 & m_z & 0 & -ma_x & 0 \\ 0 & -ma_z & 0 & J_x & 0 & -J_{xz} \\ ma_z & 0 & -ma_x & 0 & J_y & 0 \\ 0 & ma_x & 0 & -J_{xz} & 0 & J_z \end{bmatrix} \begin{bmatrix} \dot{u} \\ \dot{v} \\ \dot{w} \\ \dot{p} \\ \dot{q} \\ \dot{r} \end{bmatrix} = F_d \qquad (5)$$

and, expanding the right hand side of equation (5),

$$\mathbf{M} \begin{bmatrix} \dot{u} \\ \dot{v} \\ \dot{w} \\ \dot{p} \\ \dot{q} \\ \dot{r} \end{bmatrix} = \mathbf{D}(u,v,w,p,q,r) + \mathbf{A}(u,v,w,p,q,r) + \mathbf{G}(\lambda_{31},\lambda_{32},\lambda_{33}) + \mathbf{P} \qquad (6)$$

Where,

$\mathbf{D}(u,v,w,p,q,r)$	is the 6×1 *dynamics* vector
$\mathbf{A}(u,v,w,p,q,r)$	is the 6×1 *aerodynamics* vector.
$\mathbf{G}(\lambda_{31},\lambda_{32},\lambda_{33})$	is the 6×1 *gravitational* and *buoyancy* vector.
$\mathbf{P}$	is the 6×1 *propulsion* vector.
$\mathbf{M}$	is the *mass* matrix.

The elements in the mass matrix **M** comprise both physical mass and inertia terms and virtual mass and inertia terms. The choice of body axis system and the symmetry of the airship ensures that some terms in the mass matrix are insignificantly small, or zero. The non-zero terms are defined as follows;

Mass m, cg coordinates in body axes (a_x, a_y, a_z), and $a_y = 0$ since the airship is symmetric.

Components of apparent mass

$$\begin{aligned} m_x &= m - X_{\dot{u}} \\ m_y &= m - Y_{\dot{v}} \\ m_z &= m - Z_{\dot{w}} \end{aligned} \tag{7}$$

where, $X_{\dot{u}}$, $Y_{\dot{v}}$ and $Z_{\dot{w}}$ are the aerodynamic derivatives which quantify virtual mass.

Components of apparent inertia

$$\begin{aligned} J_x &= I_x - L_{\dot{p}} \\ J_y &= I_y - M_{\dot{q}} \\ J_z &= I_z - N_{\dot{r}} \\ J_{xz} &= I_{xz} + N_{\dot{p}} = I_{xz} + L_{\dot{r}} \end{aligned} \tag{8}$$

where, I_x, I_y and I_z are moments of inertia about the axes *ox*, *oy* and *oz* respectively. I_{xz} is the only non-zero product of inertia. $L_{\dot{p}}$, $L_{\dot{r}}$, $M_{\dot{q}}$, $N_{\dot{p}}$ and $N_{\dot{r}}$ are the aerodynamic derivatives which quantify virtual inertia. For a buoyant vehicle like the airship for which the displaced air mass is similar to the mass of the vehicle, these non-zero virtual mass and inertia terms are significant. For example, the apparent mass of the vehicle is about 50% greater than the physical mass.

The ACSL simulation model implemented and solved the above non-linear equations as described by Gomes[1], and the vectors **D**, **A**, **G** and **P** included full non-linear elements as appropriate. The linear equations of motion used in the analysis were obtained from the ACSL simulation by invoking the ANALYSE function to linearise the solution about a chosen operating point - velocity in this instance.

Appendix 2: Review of Lipscombe's analysis

A2.1 Background

Lipscombe[3] wrote three unpublished papers in 1988 in which he analysed the longitudinal and lateral-directional stability modes of the airship at hover and at various flight speeds. The object of the papers was to find approximate expressions for the stability modes in terms of aerodynamic stability derivatives. The assumptions he made were founded on an analysis of an aerodynamic data base which was less accurate and less complete than that which subsequently became available for the YEZ-2A airship. In light of the availability of a better aerodynamic data base, it became clear that some of his assumptions concerning, in particular, the lateral-directional stability modes, especially the defining matrix approximations, were no longer valid. The following is a revision and summary of the calculations originally made by Lipscombe.

A2.2- Approximate models of the longitudinal stability modes

Lipscombe analysed the longitudinal stability modes for higher speed flight conditions by observing the numerical behaviour of the stability and control derivatives. The purpose of this paragraph is to demonstrate that the same result may be obtained by analysis.

The longitudinal state equation, assuming controls fixed, may be written,

$$\begin{bmatrix} \dot{u} \\ \dot{w} \\ \dot{q} \\ \dot{\theta} \end{bmatrix} = \mathbf{A} \begin{bmatrix} u \\ w \\ q \\ \theta \end{bmatrix} \tag{9}$$

The stability modes are characterised by the zeros of the characteristic polynomial,

$$\Delta(s) = \det[s\mathbf{I} - \mathbf{A}] \tag{10}$$

and, with reference to the longitudinal state models given in Appendix 3, the state matrix may be simplified by omitting insignificant elements to,

$$\mathbf{A} = \begin{bmatrix} x_u & x_w & x_q & x_\theta \\ 0 & z_w & z_q & z_\theta \\ 0 & m_w & m_q & m_\theta \\ 0 & 0 & 1 & 0 \end{bmatrix} \tag{11}$$

Whence, the approximate longitudinal characteristic polynomial may be written,

$$\Delta(s) \cong (s - x_u)\left(s^3 - (m_q + z_w)s^2 + (m_q z_w - m_w z_q - m_\theta)s + (m_\theta z_w - m_w z_\theta)\right) \qquad (12)$$

The third order factor may itself be factored to give,

$$\Delta(s) = (s - x_u)(s + a)(s^2 + bs + c) \qquad (13)$$

whence,

$$\begin{aligned} a + b &= -(m_q + z_w) \\ ab + c &= m_q z_w - m_w z_q - m_\theta \\ ac &= m_\theta z_w - m_w z_\theta \end{aligned} \qquad (14)$$

At an initial speed of 30 m/s the values of the derivatives are such that, typically, c=0.05ab. Thus, it is reasonable to assume that ab>>c, then it may be shown that,

$$a^2 + (m_q + z_w)a + (m_q z_w - m_w z_q - m_\theta) = 0 \qquad (15)$$

with solution,

$$a = \frac{1}{2}\left\{-(m_q + z_w) \pm (m_q - z_w)\sqrt{1 + \frac{4(m_w z_q + m_\theta)}{(m_q - z_w)^2}}\right\} \qquad (16)$$

For all speeds from the hover the square root term is approximately equal to 1, for example at a speed of 30 m/s the square root is equal to 1.06. Thus,

$$a = -m_q \quad \text{or} \quad a = -z_w$$

In fact, it is found that $a \cong -z_w$ at the very lowest speeds and $a \cong -m_q$ at higher speeds where aerodynamic damping becomes effective.

Thus, at very low speeds the complete solution is,

$$a = -z_w \qquad b = -m_q \qquad c = \frac{m_w z_\theta}{z_w} - m_\theta$$

and the approximate factors of the longitudinal characteristic polynomial may be written,

$$\begin{aligned} \Delta(s) &\cong (s - x_u)(s - z_w)\left(s^2 - m_q s + \left(\frac{m_w z_\theta}{z_w} - m_\theta\right)\right) \\ &\cong (s - x_u)(s - z_w)(s^2 - m_q s - m_\theta) \end{aligned} \qquad (17)$$

Since, at low speed $m_\theta >> \frac{m_w z_\theta}{z_w}$.

Thus, to a good approximation the low speed longitudinal stability modes are characterised as follows;

Speed subsidence, or surge mode $(s - x_u)$

Heave subsidence mode, $(s - z_w)$

Longitudinal pendulum mode $(s^2 - m_q s - m_\theta)$

At moderate and higher speeds the complete solution is,

$$a = -m_q \quad b = -z_w \quad c = \frac{m_w z_\theta - m_\theta z_w}{m_q}$$

and the approximate factors of the longitudinal characteristic polynomial may be written,

$$\begin{aligned} \Delta(s) &\cong (s - x_u)(s - m_q)\left(s^2 - z_w s + \left(\frac{m_w z_\theta - m_\theta z_w}{m_q}\right)\right) \\ &\cong (s - x_u)(s - m_q)\left(s^2 - z_w s - \frac{m_\theta z_w}{m_q}\right) \end{aligned} \tag{18}$$

Since, at high speed $m_\theta z_w >> m_w z_\theta$.

Thus, to a good approximation the high speed longitudinal stability modes are characterised as follows;

Speed subsidence, or surge mode $(s - x_u)$

Pitch subsidence mode $(s - m_q)$

Longitudinal pendulum mode $\left(s^2 - z_w s - \frac{m_\theta z_w}{m_q}\right)$

A2.3 Approximate models of the lateral-directional stability modes

The lateral-directional state equation, assuming controls fixed, may be written,

$$\begin{bmatrix} \dot{v} \\ \dot{p} \\ \dot{r} \\ \dot{\phi} \end{bmatrix} = \mathbf{A} \begin{bmatrix} v \\ p \\ r \\ \phi \end{bmatrix} \tag{19}$$

The stability modes are characterised by the zeros of the characteristic polynomial,

$$\Delta(s) = \det[s\mathbf{I} - \mathbf{A}] \tag{20}$$

Analysis of the lateral-directional state matrices obtained from the ACSL simulation, as set out in Appendix 3, suggests that the state matrix may be simplified by omitting insignificant elements to,

$$\mathbf{A} = \begin{bmatrix} y_v & y_p & y_r & y_\phi \\ l_v & l_p & l_r & l_\phi \\ 0 & 0 & n_r & 0 \\ 0 & 1 & 0 & 0 \end{bmatrix} \tag{21}$$

Whence, the characteristic polynomial may be written,

$$\Delta(s) \cong (s - n_r)\left(s^3 - (l_p + y_v)s^2 - (l_\phi + l_v y_p - l_p y_v)s + (l_\phi y_v - l_v y_\phi)\right) \tag{22}$$

It is possible to simplify the characteristic polynomial further since, for all flight conditions, it may be shown that,

$$l_p >> y_v \quad \text{and} \quad l_\phi >> l_v y_p - l_p y_v$$

whence,

$$\Delta(s) \cong (s - n_r)\left(s^3 - l_p s^2 - l_\phi s + (l_\phi y_v - l_v y\phi)\right) \tag{23}$$

As before, the third order factor may itself be factored to give,

$$\Delta(s) = (s - n_r)(s + a)(s^2 + bs + c) \tag{24}$$

whence,

$$\begin{aligned} a + b &= -l_p \\ ab + c &= -l_\phi \\ ac &= l_\phi y_v - l_v y_\phi \end{aligned} \tag{25}$$

If it is assumed that $c >> ab$, then it follows that,

$$\Delta(s) \cong (s - n_r)\left(s + y_v - \frac{l_v y_\phi}{l_\phi}\right)\left(s^2 - \left(l_p + y_v - \frac{l_v y_\phi}{l_\phi}\right)s - l_\phi\right) \tag{26}$$

Thus, to a good approximation the lateral-directional stability modes are characterised as follows;

Yaw subsidence mode $\left(s - n_r\right)$

Sideslip subsidence mode $\left(s + y_v - \frac{l_v y_\phi}{l_\phi}\right)$

Oscillatory roll mode $\left(s^2 - \left(l_p + y_v - \frac{l_v y_\phi}{l_\phi}\right)s - l_\phi\right)$

Appendix 3: State space models and response transfer functions

(i) The linear state space equations were obtained directly from the non-linear ACSL simulation by linearising about a chosen trim speed.

(ii) Note that terms in the **A** and **B** matrices like 0.000 denotes a very small, but generally non-zero, number. MATLAB computations retained the actual values of such small numbers.

(iii) Neutral buoyancy is assumed.

(iv) The nominal mass of the airship is 87000 kg.

A3.1 Longitudinal models

Thrust control transfer functions are not shown.

§ State space model for $U_0 = 30$ m / sec

$$\begin{bmatrix} \dot{u} \\ \dot{w} \\ \dot{q} \\ \dot{\theta} \end{bmatrix} = \begin{bmatrix} -0.0339 & -0.0516 & 12.4561 & 0.8269 \\ 0.0007 & -0.2166 & 37.3577 & -0.0161 \\ 0.0001 & 0.0037 & -1.3048 & -0.0860 \\ 0 & 0 & 1 & 0 \end{bmatrix} \begin{bmatrix} u \\ w \\ q \\ \theta \end{bmatrix} + \begin{bmatrix} 0.0154 & 0.0000 \\ -0.0293 & 0.0000 \\ -0.0016 & 0.0000 \\ 0 & 0 \end{bmatrix} \begin{bmatrix} \delta_e \\ \delta_t \end{bmatrix}$$

Elevator response transfer functions,

$$\frac{u(s)}{\delta_e(s)} = \frac{N_{\delta_e}^{u}(s)}{\Delta(s)} = \frac{0.0154(s+0.027)(s^2+0.2988s+0.0964)}{(s+0.0326)(s+1.3638)(s^2+0.1588s+0.0138)} \quad \frac{\text{m/s}}{\text{rad}}$$

$$\frac{w(s)}{\delta_e(s)} = \frac{N_{\delta_e}^{w}(s)}{\Delta(s)} = \frac{-0.0293(s+0.0257)(s+0.0327)(s+3.3131)}{(s+0.0326)(s+1.3638)(s^2+0.1588s+0.0138)} \quad \frac{\text{m/s}}{\text{rad}}$$

$$\frac{q(s)}{\delta_e(s)} = \frac{N_{\delta_e}^{q}(s)}{\Delta(s)} = \frac{-0.0016s(s+0.0326)(s+0.2849)}{(s+0.0326)(s+1.3638)(s^2+0.1588s+0.0138)} \quad \frac{\text{rad/s}}{\text{rad}}$$

$$\frac{\theta(s)}{\delta_e(s)} = \frac{N_{\delta_e}^{\theta}(s)}{\Delta(s)} = \frac{-0.0016(s+0.0326)(s+0.2849)}{(s+0.0326)(s+1.3638)(s^2+0.1588s+0.0138)} \quad \frac{\text{rad}}{\text{rad}}$$

§ State space model for $U_0 = 25$ m / sec

$$\begin{bmatrix} \dot{u} \\ \dot{w} \\ \dot{q} \\ \dot{\theta} \end{bmatrix} = \begin{bmatrix} -0.0283 & -0.0434 & 10.3961 & 0.8266 \\ 0.0006 & -0.1807 & 31.2069 & -0.0102 \\ 0.0001 & 0.0031 & -1.0880 & -0.0860 \\ 0 & 0 & 1 & 0 \end{bmatrix} \begin{bmatrix} u \\ w \\ q \\ \theta \end{bmatrix} + \begin{bmatrix} 0.0106 & 0.0000 \\ -0.0200 & 0.0000 \\ -0.0011 & 0.0000 \\ 0 & 0 \end{bmatrix} \begin{bmatrix} \delta_e \\ \delta_t \end{bmatrix}$$

Elevator response transfer functions,

$$\frac{u(s)}{\delta_e(s)} = \frac{N_{\delta_e}^{u}(s)}{\Delta(s)} = \frac{0.0106(s+0.0332)(s^2+0.2354s+0.0652)}{(s+0.0272)(s+1.1159)(s^2+0.1538s+0.0140)} \quad \frac{\text{m/s}}{\text{rad}}$$

$$\frac{w(s)}{\delta_e(s)} = \frac{N_{\delta_e}^{w}(s)}{\Delta(s)} = \frac{-0.0200(s+0.0273)(s+0.0308)(s+2.7723)}{(s+0.0272)(s+1.1159)(s^2+0.1538s+0.0140)} \quad \frac{\text{m/s}}{\text{rad}}$$

$$\frac{q(s)}{\delta_e(s)} = \frac{N_{\delta_e}^{q}(s)}{\Delta(s)} = \frac{-0.0011s(s+0.0272)(s+0.2374)}{(s+0.0272)(s+1.1159)(s^2+0.1538s+0.0140)} \quad \frac{\text{rad/s}}{\text{rad}}$$

$$\frac{\theta(s)}{\delta_e(s)} = \frac{N_{\delta_e}^{\theta}(s)}{\Delta(s)} = \frac{-0.0011(s+0.0272)(s+0.2374)}{(s+0.0272)(s+1.1159)(s^2+0.1538s+0.0140)} \quad \frac{\text{rad}}{\text{rad}}$$

§ State space model for $U_0 = 20$ m / sec

$$\begin{bmatrix} \dot{u} \\ \dot{w} \\ \dot{q} \\ \dot{\theta} \end{bmatrix} = \begin{bmatrix} -0.0226 & -0.0350 & 8.3287 & 0.8264 \\ 0.0005 & -0.1447 & 25.0153 & -0.0054 \\ 0.0001 & 0.0025 & -0.8709 & -0.0860 \\ 0 & 0 & 1 & 0 \end{bmatrix} \begin{bmatrix} u \\ w \\ q \\ \theta \end{bmatrix} + \begin{bmatrix} 0.0068 & 0.0000 \\ -0.0128 & 0.0000 \\ -0.0007 & 0.0000 \\ 0 & 0 \end{bmatrix} \begin{bmatrix} \delta_e \\ \delta_t \end{bmatrix}$$

Elevator response transfer functions,

$$\frac{u(s)}{\delta_e(s)} = \frac{N_{\delta_e}^{u}(s)}{\Delta(s)} = \frac{0.0068(s+0.0438)(s^2+0.1692s+0.0396)}{(s+0.0218)(s+0.8593)(s^2+0.1570s+0.0145)} \quad \frac{\text{m / s}}{\text{rad}}$$

$$\frac{w(s)}{\delta_e(s)} = \frac{N_{\delta_e}^{w}(s)}{\Delta(s)} = \frac{-0.0128(s+0.0218)(s+0.0386)(s+2.2200)}{(s+0.0218)(s+0.8593)(s^2+0.1570s+0.0145)} \quad \frac{\text{m / s}}{\text{rad}}$$

$$\frac{q(s)}{\delta_e(s)} = \frac{N_{\delta_e}^{q}(s)}{\Delta(s)} = \frac{-0.0007s(s+0.0217)(s+0.1898)}{(s+0.0218)(s+0.8593)(s^2+0.1570s+0.0145)} \quad \frac{\text{rad / s}}{\text{rad}}$$

$$\frac{\theta(s)}{\delta_e(s)} = \frac{N_{\delta_e}^{\theta}(s)}{\Delta(s)} = \frac{-0.0007(s+0.0217)(s+0.1898)}{(s+0.0218)(s+0.8593)(s^2+0.1570s+0.0145)} \quad \frac{\text{rad}}{\text{rad}}$$

§ State space model for $U_0 = 12$ m / sec

$$\begin{bmatrix} \dot{u} \\ \dot{w} \\ \dot{q} \\ \dot{\theta} \end{bmatrix} = \begin{bmatrix} -0.0135 & -0.0212 & 5.0073 & 0.8262 \\ 0.0003 & -0.0869 & 15.0435 & 0.0002 \\ 0.0000 & 0.0015 & -0.5229 & -0.0859 \\ 0 & 0 & 1 & 0 \end{bmatrix} \begin{bmatrix} u \\ w \\ q \\ \theta \end{bmatrix} + \begin{bmatrix} 0.0025 & 0.0000 \\ -0.0046 & 0.0000 \\ -0.0003 & 0.0000 \\ 0 & 0 \end{bmatrix} \begin{bmatrix} \delta_e \\ \delta_t \end{bmatrix}$$

Elevator response transfer functions,

$$\frac{u(s)}{\delta_e(s)} = \frac{N_{\delta_e}^{u}(s)}{\Delta(s)} = \frac{0.0025(s+0.0806)(s^2+0.0478s+0.0133)}{(s+0.0131)(s+0.3722)(s^2+0.238s+0.0201)} \quad \frac{\text{m / s}}{\text{rad}}$$

$$\frac{w(s)}{\delta_e(s)} = \frac{N_{\delta_e}^{w}(s)}{\Delta(s)} = \frac{-0.0046(s+0.0131)(s+0.0665)(s+1.2915)}{(s+0.031)(s+0.3722)(s^2+0.238s+0.0201)} \quad \frac{\text{m / s}}{\text{rad}}$$

$$\frac{q(s)}{\delta_e(s)} = \frac{N_{\delta_e}^{q}(s)}{\Delta(s)} = \frac{-0.0003s(s+0.0130)(s+0.1142)}{(s+0.031)(s+0.3722)(s^2+0.238s+0.0201)} \quad \frac{\text{rad / s}}{\text{rad}}$$

$$\frac{\theta(s)}{\delta_e(s)} = \frac{N_{\delta_e}^{\theta}(s)}{\Delta(s)} = \frac{-0.0003(s+0.0130)(s+0.1142)}{(s+0.031)(s+0.3722)(s^2+0.238s+0.0201)} \quad \frac{\text{rad}}{\text{rad}}$$

§ State space model for $U_0 = 8$ m / sec

$$\begin{bmatrix} \dot{u} \\ \dot{w} \\ \dot{q} \\ \dot{\theta} \end{bmatrix} = \begin{bmatrix} -0.0090 & -0.0141 & 3.3425 & 0.8261 \\ 0.0002 & -0.0580 & 10.0361 & 0.0019 \\ 0.0000 & 0.0010 & -0.3487 & -0.0859 \\ 0 & 0 & 1 & 0 \end{bmatrix} \begin{bmatrix} u \\ w \\ q \\ \theta \end{bmatrix} + \begin{bmatrix} 0.0011 & 0.0000 \\ -0.0020 & 0.0000 \\ -0.0001 & 0.0000 \\ 0 & 0 \end{bmatrix} \begin{bmatrix} \delta_e \\ \delta_t \end{bmatrix}$$

Elevator response transfer functions,

$$\frac{u(s)}{\delta_e(s)} = \frac{N_{\delta_e}^{u}(s)}{\Delta(s)} = \frac{0.0011(s+0.0895)(s^2+0.0040s+0.0080)}{(s+0.0087)(s+0.0683)(s^2+0.3386s+0.0729)} \quad \frac{\text{m/s}}{\text{rad}}$$

$$\frac{w(s)}{\delta_e(s)} = \frac{N_{\delta_e}^{w}(s)}{\Delta(s)} = \frac{-0.0020(s+0.0087)(s+0.1076)(s+0.7994)}{(s+0.0087)(s+0.0683)(s^2+0.3386s+0.0729)} \quad \frac{\text{m/s}}{\text{rad}}$$

$$\frac{q(s)}{\delta_e(s)} = \frac{N_{\delta_e}^{q}(s)}{\Delta(s)} = \frac{-0.0001s(s+0.0087)(s+0.0761)}{(s+0.0087)(s+0.0683)(s^2+0.3386s+0.0729)} \quad \frac{\text{rad/s}}{\text{rad}}$$

$$\frac{\theta(s)}{\delta_e(s)} = \frac{N_{\delta_e}^{\theta}(s)}{\Delta(s)} = \frac{-0.0001(s+0.0087)(s+0.0761)}{(s+0.0087)(s+0.0683)(s^2+0.3386s+0.0729)} \quad \frac{\text{rad}}{\text{rad}}$$

§ State space model for $U_0 = 3$ m / sec

$$\begin{bmatrix} \dot{u} \\ \dot{w} \\ \dot{q} \\ \dot{\theta} \end{bmatrix} = \begin{bmatrix} -0.0034 & -0.0053 & 1.2564 & 0.8260 \\ 0.0001 & -0.0217 & 3.7654 & 0.0030 \\ 0.0000 & 0.0004 & -0.1308 & -0.0859 \\ 0 & 0 & 1 & 0 \end{bmatrix} \begin{bmatrix} u \\ w \\ q \\ \theta \end{bmatrix} + 10^{-3} \times \begin{bmatrix} 0.1528 & 0.0096 \\ -0.2838 & 0.0000 \\ -0.0160 & 0.0001 \\ 0 & 0 \end{bmatrix} \begin{bmatrix} \delta_e \\ \delta_t \end{bmatrix}$$

Elevator response transfer functions,

$$\frac{u(s)}{\delta_e(s)} = \frac{N_{\delta_e}^{u}(s)}{\Delta(s)} = \frac{0.1528 \times 10^{-3}(s+0.0730)(s^2+0.0424s+0.0034)}{(s+0.0033)(s+0.0221)(s^2+0.1306s+0.0845)} \quad \frac{\text{m/s}}{\text{rad}}$$

$$\frac{w(s)}{\delta_e(s)} = \frac{N_{\delta_e}^{w}(s)}{\Delta(s)} = \frac{-0.2838 \times 10^{-3}(s+0.0033)(s^2+0.3436s+0.0861)}{(s+0.0033)(s+0.0221)(s^2+0.1306s+0.0845)} \quad \frac{\text{m/s}}{\text{rad}}$$

$$\frac{q(s)}{\delta_e(s)} = \frac{N_{\delta_e}^{q}(s)}{\Delta(s)} = \frac{-0.0160 \times 10^{-3}s(s+0.0033)(s+0.0285)}{(s+0.0033)(s+0.0221)(s^2+0.1306s+0.0845)} \quad \frac{\text{rad/s}}{\text{rad}}$$

$$\frac{\theta(s)}{\delta_e(s)} = \frac{N_{\delta_e}^{\theta}(s)}{\Delta(s)} = \frac{-0.0160 \times 10^{-3}(s+0.0033)(s+0.0285)}{(s+0.0033)(s+0.0221)(s^2+0.1306s+0.0845)} \quad \frac{\text{rad}}{\text{rad}}$$

§ State space model for $U_0 = 1$ m / sec

$$\begin{bmatrix} \dot{u} \\ \dot{w} \\ \dot{q} \\ \dot{\theta} \end{bmatrix} = \begin{bmatrix} -0.0011 & -0.0011 & 0.4192 & 0.8260 \\ 0.0000 & -0.0072 & 1.2553 & 0.0032 \\ 0.0000 & 0.0001 & -0.0436 & -0.0859 \\ 0 & 0 & 1 & 0 \end{bmatrix} \begin{bmatrix} u \\ w \\ q \\ \theta \end{bmatrix} + 10^{-4} \times \begin{bmatrix} 0.1728 & 0.0964 \\ -0.3138 & 0.0000 \\ -0.0176 & 0.0010 \\ 0 & 0 \end{bmatrix} \begin{bmatrix} \delta_e \\ \delta_t \end{bmatrix}$$

Elevator response transfer functions,

$$\frac{u(s)}{\delta_e(s)} = \frac{N_{\delta_e}^{u}(s)}{\Delta(s)} = \frac{0.1728 \times 10^{-4}(s - 0.0066)(s^2 + 0.0166s + 0.0018)}{(s + 0.0011)(s + 0.0072)(s^2 + 0.0436s + 0.0857)} \quad \frac{\text{m / s}}{\text{rad}}$$

$$\frac{w(s)}{\delta_e(s)} = \frac{N_{\delta_e}^{w}(s)}{\Delta(s)} = \frac{-0.3138 \times 10^{-4}(s + 0.0011)(s^2 + 0.1142s + 0.0861)}{(s + 0.0011)(s + 0.0072)(s^2 + 0.0436s + 0.0857)} \quad \frac{\text{m / s}}{\text{rad}}$$

$$\frac{q(s)}{\delta_e(s)} = \frac{N_{\delta_e}^{q}(s)}{\Delta(s)} = \frac{-0.0176 \times 10^{-4} s(s + 0.0011)(s + 0.0095)}{(s + 0.0011)(s + 0.0072)(s^2 + 0.0436s + 0.0857)} \quad \frac{\text{rad / s}}{\text{rad}}$$

$$\frac{\theta(s)}{\delta_e(s)} = \frac{N_{\delta_e}^{\theta}(s)}{\Delta(s)} = \frac{-0.0176 \times 10^{-4}(s + 0.0011)(s + 0.0095)}{(s + 0.0011)(s + 0.0072)(s^2 + 0.0436s + 0.0857)} \quad \frac{\text{rad}}{\text{rad}}$$

§ State space model for $U_0 = 0.1$ m / sec (Hover)

$$\begin{bmatrix} \dot{u} \\ \dot{w} \\ \dot{q} \\ \dot{\theta} \end{bmatrix} = \begin{bmatrix} -0.0001 & -0.0001 & 0.0421 & 0.8260 \\ 0.0000 & -0.0007 & 0.1256 & 0.0032 \\ 0.0000 & 0.0000 & -0.0044 & -0.0859 \\ 0 & 0 & 1 & 0 \end{bmatrix} \begin{bmatrix} u \\ w \\ q \\ \theta \end{bmatrix} + 10^{-5} \times \begin{bmatrix} 0.0000 & 0.9641 \\ -0.0341 & -0.0004 \\ 0.0000 & 0.0101 \\ 0 & 0 \end{bmatrix} \begin{bmatrix} \delta_e \\ \delta_t \end{bmatrix}$$

Elevator response transfer functions,

$$\frac{u(s)}{\delta_e(s)} = \frac{N_{\delta_e}^{u}(s)}{\Delta(s)} = \frac{0.0000 \times 10^{-6} s(s - 0.2191)(s + 0.2166)}{(s + 0.0001)(s + 0.0007)(s^2 + 0.0044s + 0.0859)} \quad \frac{\text{m / s}}{\text{rad}}$$

$$\frac{w(s)}{\delta_e(s)} = \frac{N_{\delta_e}^{w}(s)}{\Delta(s)} = \frac{-0.3411 \times 10^{-6}(s + 0.0001)(s^2 + 0.0044s + 0.0859)}{(s + 0.0001)(s + 0.0007)(s^2 + 0.0044s + 0.0859)} \quad \frac{\text{m / s}}{\text{rad}}$$

$$\frac{q(s)}{\delta_e(s)} = \frac{N_{\delta_e}^{q}(s)}{\Delta(s)} = \frac{0.0000 \times 10^{-6} s^2(s + 0.0001)}{(s + 0.0001)(s + 0.0007)(s^2 + 0.0044s + 0.0859)} \quad \frac{\text{rad / s}}{\text{rad}}$$

$$\frac{\theta(s)}{\delta_e(s)} = \frac{N_{\delta_e}^{\theta}(s)}{\Delta(s)} = \frac{0.0000 \times 10^{-6} s(s + 0.0001)}{(s + 0.0001)(s + 0.0007)(s^2 + 0.0044s + 0.0859)} \quad \frac{\text{rad}}{\text{rad}}$$

A3.2 Lateral-directional models

§ State space model for $U_0 = 30$ m / sec

$$\begin{bmatrix} \dot{v} \\ \dot{p} \\ \dot{r} \\ \dot{\phi} \end{bmatrix} = \begin{bmatrix} 0.0931 & -2.0392 & 12.3546 & -2.9512 \\ 0.0490 & -0.3758 & 1.6514 & -0.5277 \\ -0.0054 & -0.0055 & -1.3979 & -0.0044 \\ 0 & 1 & 0 & 0 \end{bmatrix} \begin{bmatrix} v \\ p \\ r \\ \phi \end{bmatrix} + \begin{bmatrix} 0.0455 \\ 0.0026 \\ -0.0023 \\ 0 \end{bmatrix} \delta_r$$

Rudder response transfer functions,

$$\frac{v(s)}{\delta_r(s)} = \frac{N_{\delta_r}^{v}(s)}{\Delta(s)} = \frac{0.0455(s+0.8451)(s^2+0.1918s+0.5031)}{(s+0.1811)(s+1.3498)(s^2+0.1496s+0.5904)} \quad \frac{\text{m/s}}{\text{rad}}$$

$$\frac{p(s)}{\delta_r(s)} = \frac{N_{\delta_r}^{p}(s)}{\Delta(s)} = \frac{0.0026s(s^2+0.7042s+0.4635)}{(s+0.1811)(s+1.3498)(s^2+0.1496s+0.5904)} \quad \frac{\text{rad/s}}{\text{rad}}$$

$$\frac{r(s)}{\delta_r(s)} = \frac{N_{\delta_r}^{r}(s)}{\Delta(s)} = \frac{-0.0023(s+0.2333)(s^2+0.1636s+0.5922)}{(s+0.1811)(s+1.3498)(s^2+0.1496s+0.5904)} \quad \frac{\text{rad/s}}{\text{rad}}$$

$$\frac{\phi(s)}{\delta_r(s)} = \frac{N_{\delta_r}^{\phi}(s)}{\Delta(s)} = \frac{0.0026(s^2+0.7042s+0.4635)}{(s+0.1811)(s+1.3498)(s^2+0.1496s+0.5904)} \quad \frac{\text{rad}}{\text{rad}}$$

§ State space model for $U_0 = 25$ m / sec

$$\begin{bmatrix} \dot{v} \\ \dot{p} \\ \dot{r} \\ \dot{\phi} \end{bmatrix} = \begin{bmatrix} 0.0765 & -1.7072 & 10.1930 & -2.9511 \\ 0.0408 & -0.3132 & 1.3723 & -0.5277 \\ -0.0045 & -0.0048 & -1.1612 & -0.0058 \\ 0 & 1 & 0 & 0 \end{bmatrix} \begin{bmatrix} v \\ p \\ r \\ \phi \end{bmatrix} + \begin{bmatrix} 0.0306 \\ 0.0016 \\ -0.0016 \\ 0 \end{bmatrix} \delta_r$$

Rudder response transfer functions,

$$\frac{v(s)}{\delta_r(s)} = \frac{N_{\delta_r}^{v}(s)}{\Delta(s)} = \frac{0.0306(s+0.7326)(s^2+0.1212s+0.4993)}{(s+0.1550)(s+1.1259)(s^2+0.1170s+0.5765)} \quad \frac{\text{m/s}}{\text{rad}}$$

$$\frac{p(s)}{\delta_r(s)} = \frac{N_{\delta_r}^{p}(s)}{\Delta(s)} = \frac{0.0016s(s^2+0.5116s+0.4260)}{(s+0.1550)(s+1.1259)(s^2+0.1170s+0.5765)} \quad \frac{\text{rad/s}}{\text{rad}}$$

$$\frac{r(s)}{\delta_r(s)} = \frac{N_{\delta_r}^{r}(s)}{\Delta(s)} = \frac{-0.0016(s+0.2019)(s^2+0.1270s+0.5765)}{(s+0.1550)(s+1.1259)(s^2+0.1170s+0.5765)} \quad \frac{\text{rad/s}}{\text{rad}}$$

$$\frac{\phi(s)}{\delta_r(s)} = \frac{N_{\delta_r}^{\phi}(s)}{\Delta(s)} = \frac{0.0016(s^2+0.5116s+0.4260)}{(s+0.1550)(s+1.1259)(s^2+0.1170s+0.5765)} \quad \frac{\text{rad}}{\text{rad}}$$

§ State space model for $U_0 = 20$ m / sec

$$\begin{bmatrix} \dot{v} \\ \dot{p} \\ \dot{r} \\ \dot{\phi} \end{bmatrix} = \begin{bmatrix} 0.0609 & -1.3718 & 8.0877 & -2.9513 \\ 0.0326 & -0.2507 & 1.0953 & -0.5277 \\ -0.0036 & -0.0040 & -0.9266 & -0.0070 \\ 0 & 1 & 0 & 0 \end{bmatrix} \begin{bmatrix} v \\ p \\ r \\ \phi \end{bmatrix} + \begin{bmatrix} 0.0189 \\ 0.0009 \\ -0.0010 \\ 0 \end{bmatrix} \delta_r$$

Rudder response transfer functions,

$$\frac{v(s)}{\delta_r(s)} = \frac{N_{\delta_r}^{v}(s)}{\Delta(s)} = \frac{0.0189(s+0.6175)(s^2+0.0568s+0.4900)}{(s+0.1264)(s+0.9039)(s^2+0.0860s+0.5636)} \quad \frac{\text{m / s}}{\text{rad}}$$

$$\frac{p(s)}{\delta_r(s)} = \frac{N_{\delta_r}^{p}(s)}{\Delta(s)} = \frac{0.0009s(s^2+0.3348s+0.2883)}{(s+0.1264)(s+0.9039)(s^2+0.0860s+0.5636)} \quad \frac{\text{rad / s}}{\text{rad}}$$

$$\frac{r(s)}{\delta_r(s)} = \frac{N_{\delta_r}^{r}(s)}{\Delta(s)} = \frac{-0.0010(s+0.1662)(s^2+0.0944s+0.5623)}{(s+0.1264)(s+0.9039)(s^2+0.0860s+0.5636)} \quad \frac{\text{rad / s}}{\text{rad}}$$

$$\frac{\phi(s)}{\delta_r(s)} = \frac{N_{\delta_r}^{\phi}(s)}{\Delta(s)} = \frac{0.0009(s^2+0.3348s+0.2883)}{(s+0.1264)(s+0.9039)(s^2+0.0860s+0.5636)} \quad \frac{\text{rad}}{\text{rad}}$$

§ State space model for $U_0 = 12$ m / sec

$$\begin{bmatrix} \dot{v} \\ \dot{p} \\ \dot{r} \\ \dot{\phi} \end{bmatrix} = \begin{bmatrix} 0.0363 & -0.8273 & 4.8063 & -2.9516 \\ 0.0195 & -0.1504 & 0.6554 & -0.5278 \\ -0.0022 & -0.0025 & -0.5542 & -0.0084 \\ 0 & 1 & 0 & 0 \end{bmatrix} \begin{bmatrix} v \\ p \\ r \\ \phi \end{bmatrix} + \begin{bmatrix} 0.0067 \\ 0.0003 \\ -0.0004 \\ 0 \end{bmatrix} \delta_r$$

Rudder response transfer functions,

$$\frac{v(s)}{\delta_r(s)} = \frac{N_{\delta_r}^{v}(s)}{\Delta(s)} = \frac{0.0067(s+0.4157)(s^2-0.0134s+0.4439)}{(s+0.0777)(s+0.5486)(s^2+0.0420s+0.5448)} \quad \frac{\text{m / s}}{\text{rad}}$$

$$\frac{p(s)}{\delta_r(s)} = \frac{N_{\delta_r}^{p}(s)}{\Delta(s)} = \frac{0.0003s(s^2+0.1794s+0.1062)}{(s+0.0777)(s+0.5486)(s^2+0.0420s+0.5448)} \quad \frac{\text{rad / s}}{\text{rad}}$$

$$\frac{r(s)}{\delta_r(s)} = \frac{N_{\delta_r}^{r}(s)}{\Delta(s)} = \frac{-0.0004(s+0.1036)(s^2+0.0524s+0.5456)}{(s+0.0777)(s+0.5486)(s^2+0.0420s+0.5448)} \quad \frac{\text{rad / s}}{\text{rad}}$$

$$\frac{\phi(s)}{\delta_r(s)} = \frac{N_{\delta_r}^{\phi}(s)}{\Delta(s)} = \frac{0.0003(s^2+0.1794s+0.1062)}{(s+0.0777)(s+0.5486)(s^2+0.0420s+0.5448)} \quad \frac{\text{rad}}{\text{rad}}$$

§ State space model for $U_0 = 8$ m / sec

$$\begin{bmatrix} \dot{v} \\ \dot{p} \\ \dot{r} \\ \dot{\phi} \end{bmatrix} = \begin{bmatrix} 0.0240 & -0.5544 & 3.1954 & -2.9518 \\ 0.0130 & -0.1003 & 0.4366 & -0.5278 \\ -0.0014 & -0.0017 & -0.3692 & -0.0089 \\ 0 & 1 & 0 & 0 \end{bmatrix} \begin{bmatrix} v \\ p \\ r \\ \phi \end{bmatrix} + \begin{bmatrix} 0.0029 \\ 0.0001 \\ -0.0002 \\ 0 \end{bmatrix} \delta_r$$

Rudder response transfer functions,

$$\frac{v(s)}{\delta_r(s)} = \frac{N_{\delta_r}^{v}(s)}{\Delta(s)} = \frac{0.0029(s+0.2947)(s^2-0.0312s+0.4348)}{(s+0.0522)(s+0.3688)(s^2+0.0246s+0.5366)} \quad \frac{\text{m/s}}{\text{rad}}$$

$$\frac{p(s)}{\delta_r(s)} = \frac{N_{\delta_r}^{p}(s)}{\Delta(s)} = \frac{0.0001s(s^2+0.0668s+0.0517)}{(s+0.0522)(s+0.3688)(s^2+0.0246s+0.5366)} \quad \frac{\text{rad/s}}{\text{rad}}$$

$$\frac{r(s)}{\delta_r(s)} = \frac{N_{\delta_r}^{r}(s)}{\Delta(s)} = \frac{-0.0002(s+0.0699)(s^2+0.0330s+0.5392)}{(s+0.0522)(s+0.3688)(s^2+0.0246s+0.5366)} \quad \frac{\text{rad/s}}{\text{rad}}$$

$$\frac{\phi(s)}{\delta_r(s)} = \frac{N_{\delta_r}^{\phi}(s)}{\Delta(s)} = \frac{0.0001(s^2+0.0668s+0.0517)}{(s+0.0522)(s+0.3688)(s^2+0.0246s+0.5366)} \quad \frac{\text{rad}}{\text{rad}}$$

§ State space model for $U_0 = 3$ m / sec

$$\begin{bmatrix} \dot{v} \\ \dot{p} \\ \dot{r} \\ \dot{\phi} \end{bmatrix} = \begin{bmatrix} 0.0089 & -0.2099 & 1.1965 & -2.9519 \\ 0.0049 & -0.0376 & 0.1637 & -0.5278 \\ -0.0005 & -0.0006 & -0.1384 & -0.0091 \\ 0 & 1 & 0 & 0 \end{bmatrix} \begin{bmatrix} v \\ p \\ r \\ \phi \end{bmatrix} + 10^{-3} \times \begin{bmatrix} 0.3781 \\ 0.0132 \\ -0.0230 \\ 0 \end{bmatrix} \delta_r$$

Rudder response transfer functions,

$$\frac{v(s)}{\delta_r(s)} = \frac{N_{\delta_r}^{v}(s)}{\Delta(s)} = \frac{0.3781\times10^{-3}(s+0.1181)(s^2-0.0220s+0.4310)}{(s+0.0197)(s+0.1396)(s^2+0.0078s+0.5291)} \quad \frac{\text{m/s}}{\text{rad}}$$

$$\frac{p(s)}{\delta_r(s)} = \frac{N_{\delta_r}^{p}(s)}{\Delta(s)} = \frac{0.0132\times10^{-3}s(s^2-0.0162s+0.0086)}{(s+0.0197)(s+0.1396)(s^2+0.0078s+0.5291)} \quad \frac{\text{rad/s}}{\text{rad}}$$

$$\frac{r(s)}{\delta_r(s)} = \frac{N_{\delta_r}^{r}(s)}{\Delta(s)} = \frac{-0.0230\times10^{-3}(s+0.0264)(s^2+0.0116s+0.5337)}{(s+0.0197)(s+0.1396)(s^2+0.0078s+0.5291)} \quad \frac{\text{rad/s}}{\text{rad}}$$

$$\frac{\phi(s)}{\delta_r(s)} = \frac{N_{\delta_r}^{\phi}(s)}{\Delta(s)} = \frac{0.0132\times10^{-3}(s^2-0.0162s+0.0086)}{(s+0.0197)(s+0.1396)(s^2+0.0078s+0.5291)} \quad \frac{\text{rad}}{\text{rad}}$$

§ State space model for $U_0 = 1$ m / sec

$$\begin{bmatrix} \dot{v} \\ \dot{p} \\ \dot{r} \\ \dot{\phi} \end{bmatrix} = \begin{bmatrix} 0.0030 & -0.0702 & 0.3989 & -2.9519 \\ 0.0016 & -0.0125 & 0.0546 & -0.5278 \\ -0.0002 & -0.0002 & -0.0462 & -0.0092 \\ 0 & 1 & 0 & 0 \end{bmatrix} \begin{bmatrix} v \\ p \\ r \\ \phi \end{bmatrix} + 10^{-4} \times \begin{bmatrix} 0.4089 \\ 0.0127 \\ -0.0256 \\ 0 \end{bmatrix} \delta_r$$

Rudder response transfer functions,

$$\frac{v(s)}{\delta_r(s)} = \frac{N_{\delta_r}^{v}(s)}{\Delta(s)} = \frac{0.4089 \times 10^{-4}(s+0.0399)(s^2 - 0.0084s + 0.4370)}{(s+0.0066)(s+0.0466)(s^2 + 0.0026s + 0.5280)} \quad \frac{\text{m/s}}{\text{rad}}$$

$$\frac{p(s)}{\delta_r(s)} = \frac{N_{\delta_r}^{p}(s)}{\Delta(s)} = \frac{0.0127 \times 10^{-4} s(s^2 - 0.0146s + 0.0011)}{(s+0.0066)(s+0.0466)(s^2 + 0.0026s + 0.5280)} \quad \frac{\text{rad/s}}{\text{rad}}$$

$$\frac{r(s)}{\delta_r(s)} = \frac{N_{\delta_r}^{r}(s)}{\Delta(s)} = \frac{-0.0256 \times 10^{-4}(s+0.0088)(s^2 + 0.0038s + 0.5325)}{(s+0.0066)(s+0.0466)(s^2 + 0.0026s + 0.5280)} \quad \frac{\text{rad/s}}{\text{rad}}$$

$$\frac{\phi(s)}{\delta_r(s)} = \frac{N_{\delta_r}^{\phi}(s)}{\Delta(s)} = \frac{0.0127 \times 10^{-4}(s^2 - 0.0146s + 0.0011)}{(s+0.0066)(s+0.0466)(s^2 + 0.0026s + 0.5280)} \quad \frac{\text{rad}}{\text{rad}}$$

§ State space model for $U_0 = 0.1$ m / sec (Hover)

$$\begin{bmatrix} \dot{v} \\ \dot{p} \\ \dot{r} \\ \dot{\phi} \end{bmatrix} = \begin{bmatrix} -0.0054 & -0.0071 & 0.0401 & -2.9519 \\ -0.0003 & -0.0013 & 0.0055 & -0.5278 \\ 0.0002 & 0.0000 & -0.0046 & -0.0092 \\ 0 & 1 & 0 & 0 \end{bmatrix} \begin{bmatrix} v \\ p \\ r \\ \phi \end{bmatrix} + 10^{-6} \times \begin{bmatrix} 0.4058 \\ 0.0118 \\ -0.0257 \\ 0 \end{bmatrix} \delta_r$$

Rudder response transfer functions,

$$\frac{v(s)}{\delta_r(s)} = \frac{N_{\delta_r}^{v}(s)}{\Delta(s)} = \frac{0.4058 \times 10^{-6}(s+0.0040)(s^2 - 0.0008s + 0.4418)}{(s+0.0027)(s+0.0057)(s^2 + 0.0028s + 0.5278)} \quad \frac{\text{m/s}}{\text{rad}}$$

$$\frac{p(s)}{\delta_r(s)} = \frac{N_{\delta_r}^{p}(s)}{\Delta(s)} = \frac{0.0118 \times 10^{-6} s(s+0.0022)(s-0.0146)}{(s+0.0027)(s+0.0057)(s^2 + 0.0028s + 0.5278)} \quad \frac{\text{rad/s}}{\text{rad}}$$

$$\frac{r(s)}{\delta_r(s)} = \frac{N_{\delta_r}^{r}(s)}{\Delta(s)} = \frac{-0.0257 \times 10^{-6}(s+0.0011)(s^2 + 0.0026s + 0.5320)}{(s+0.0027)(s+0.0057)(s^2 + 0.0028s + 0.5278)} \quad \frac{\text{rad/s}}{\text{rad}}$$

$$\frac{\phi(s)}{\delta_r(s)} = \frac{N_{\delta_r}^{\phi}(s)}{\Delta(s)} = \frac{0.0118 \times 10^{-6}(s+0.0022)(s-0.0146)}{(s+0.0027)(s+0.0057)(s^2 + 0.0028s + 0.5278)} \quad \frac{\text{rad}}{\text{rad}}$$